ORIGINAL ARTICLE

lajss.org
Latin American Journal of Solids and Structures

www.lajss.org

Comprehensive discussion on hyperelastic orthotropic constitutive models for finite strains

Eduardo Yuiti Hayashi[a], Rodrigo Ribeiro Paccola[a], Humberto Breves Coda[a*]

[a]University of São Paulo, São Carlos, São Paulo, Brazil. Email: yuitihayashi@usp.br, rpaccola@sc.usp.br, hbcoda@sc.usp.br

*Corresponding author

https://doi.org/10.1590/1679-78258253

Abstract

In the classical literature devoted to the study of orthotropic materials under large strains, a lot of emphasis is given to strain invariants, obscuring the association of finite strain constitutive relations with well-established small strains constitutive relations. In this work, this association is established through the comparison of 8 orthotropic models (3 classical and 5 new) for hyperelastic orthotropic materials using the Flory's decomposition. This is done transforming the initial formalism of different models into complete quadratic polynomials written in terms of the Right-Cauchy-Green stretch and a volumetric control that guaranties the growth condition. A tailoring fiber-reinforced solid model - in which discrete fibers are immersed into continuous matrix - is also presented and used to establish numerical tests, generating basic elastic constants for comparisons. The 5 proposed models are implemented in an in-house FEM code and comparisons among their mechanical behavior are presented. From these comparisons one of the proposed models is selected to successfully simulate a biological tissue, opening the possibilities for future studies.

Keywords

Finite Strain, Hyperelasticity, Orthotropic Materials, Fiber reinforcement, Biomechanics

Graphical Abstract

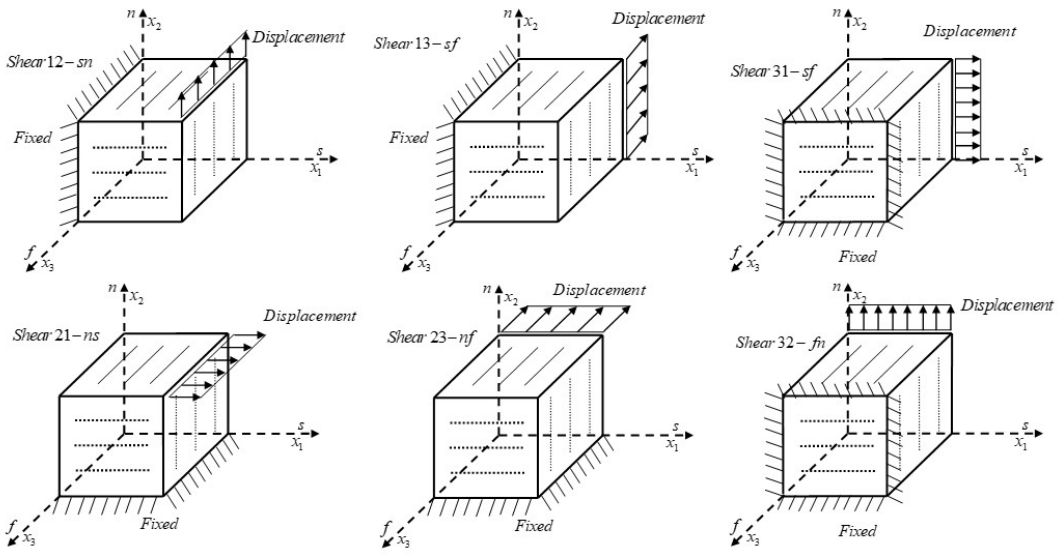

Received June 25, 2024. In revised form August 07, 2024. Accepted August 28, 2024. Available online August 30, 2024.
https://doi.org/10.1590/1679-78258253

1 INTRODUCTION

In order to associate finite strain and small strain constitutive relations and establishes a simple framework to assemble these modes, one should understand the mathematical basis of consistent models. Without intending to do an extensive review, some important studies in literature that discuss hyperelastic models for isotropic, transversally isotropic and orthotropic materials should be mentioned. One can cite theoretical studies (Rubin, 2016; Shariff, 2013; Spencer, 1984; Aguiar and Lopes da Rocha, 2018) concerned with establishing a minimum number of invariants and, therefore, a minimum number of elastic constants to be determined experimentally in order to model transversally isotropic and orthotropic materials.

Other reference studies are interested in establishing strain energy density functions that consider a larger number of elastic constants and strain invariants or their powers, seeking a better representation of complex materials such as elastomers and living tissues (Ehret and Itskov, 2007; Itskov and Khiêm, 2016; Shariff, 2022; Balzani et al., 2006). A good review on the subject can be seen, for example, in the works (Itskov and Khiêm, 2016; Shariff, 2022; Holzapfel and Ogden, 2010).

To understand the mathematical basis of consistent models one must cite the classical study (Spencer, 1984) that was concerned with the minimum number of invariants for both infinitesimal and finite strains, adopting different strain measures for each case. For infinitesimal strains, the invariants were assembled from traces of powers of the infinitesimal strain and its product with dyadics of the orthotropy directions, tabulated by Spencer (1971). For finite strains, Spencer (1984) replaced the infinitesimal strains by the Right-Cauchy-Green stretch, keeping a Lagrangian referential concluding that the minimum number of elastic constants for orthotropic materials at finite strains is 7 and for infinitesimal strains is 9. The infinitesimal result of Spencer (1984) corroborates to the consistency of linear elasticity solutions given, for example, by Lekhnitskii (1963). Related to the definition of constitutive models with a larger number of elastic constants, one can mention the study of Shariff (2022) in which the eigenvalues of strains are used to assemble strain energy densities of transversely isotropic and orthotropic materials resembling other references (Ogden, 1972; Lubarda and Chen, 2018; Schröder and Neff, 2003). In Shariff (2022) the number of elastic constants adopted for orthotropic materials in infinitesimal strains is ten, being nine called ground constants and the tenth is the bulk modulus. For finite strains Shariff (2022) proposes a strain energy density containing ten ground constants, the bulk modulus and a high-order polynomial dependent on the stretch eigenvalues.

In order to exemplify the extension of theoretical and applied studies regarding medical and engineering hyperelastic reinforced materials one may mention, among others the following authors: Jadidi et al. (2021) study the behavior of a constitutive model regarding collagen dispersion in femoral artery, Hadjicharalambous et al. (2015) compares existent orthotropic laws to define a balance among fidelity and calibration from magnetic resonance tests, Amores et al. (2021) created a non-parametric strategy to model orthotropic compressive materials based on complementary energy incrementally retrofitting results from experimental incremental steps, Sussman and Bathe (2009) and Latorre and Montáns (2014) uses logarithmic strains and splines to interpolate the elastic behavior of specific isotropic and orthotropic materials, Holzapfel and Ogden (2009) model the passive myocardium tissue proposing an important constitutive model based on strain invariants, Gao et al (2020) analyzed specific and important material in the construction industry, Yang et al (2018) analyzed the properties of fiber fabric rubber through hyper-viscoelastic constitutive model, Zhang et al (2019) applied asymptotic homogenization to describe finitely deformed heterogeneous elastomers and Sharabi et al (2016) studied the flexure behavior of bio-inspired collagen-reinforced thin composites.

In addition to the applications described above, fiber-reinforced materials that develop large strains are widely explored in the literature due to their great practical importance. Interesting research can be cited, such as the study of Zhao et al (2023) dealing with the dependence of strain rates on the rupture of fiber-reinforced polymers; the work of Gao et al (2022) which seeks to apply a specific constitutive model to the behavior of bar structures, the research of Lv et al (2024) concerned with the sliding of reinforced polymer reinforcements in relation to concrete beams. Other interesting studies are Fallahi and Taheri-Behrooz (2022) concerned with modeling the cyclic behavior of reinforced polymers and Gupta et al (2022) that uses homogenized models to simulate reinforced polymer materials manufactured by 3D printing. In order to verify the extent of this kind of application one may consult reviews as the one of Ma et al (2021) among others.

To propose and compare different hyperelastic models one starts following the hyperelastic framework of Spencer (1984), Holzapfel and Ogden (2010), Ogden (1997) and Bonet and Burton (1998) including the application of Flory's multiplicative decomposition (Flory, 1961). Fundamental aspects to capture understandings and propose evolutions are revisited. The proposed models are based on the adaptation of the isotropic strain energy densities proposed by Mooney (1940) - rewritten using isotropic strain invariants by Rivlin and Saunders (1951) - plus the volumetric part proposed by Hartmann and Neff (2003). Applying the Flory's decomposition it is possible to separate the

isochoric and volumetric parts of the Right-Cauchy-Green stretch and, as a consequence, strain energy potentials can be additively divided in volumetric and isochoric parts.

The rewritten fundamental literature models using the Flory's decomposition are: (a) Minimum parameters strain energy function, (b) Nine parameters strain energy based on orthotropic invariants and (c) Hyperelastic extension of the linear constitutive model written by Spencer (1984). These models, as well as the majority of consulted hyperelastic models for orthotropic materials, are based on the so called orthotropic invariants.

Doing a toilsome algebraic work,one analyzesthe original consistent models (a), (b) and (c) and identifies that there is a unique algebraic (polynomial) representation for these models. Thusit is concluded that the only difference among these three models the way elastic constants are grouped, which interferes in the material characterization.

At this point it is interesting to quote an affirmation of Amores et al. (2021) that there is not a phenomenological extension of the linear theory capable of effectively modeling the existing large scope of orthotropic materials at large strains. Thus, it is very important to localize our work in the effort of finding a way to extend the linear understanding of orthotropic materials to the finite strain range, at least using small strain results to assemble basic elastic constants. From this comment and the observation that models based on orthotropic invariants may be written as a simple sum of components of the Right-Cauchy-Green stretch tensor, 5 models (also making algebraic comparisons) are proposed: (d) Saint-Venant-Kirchhoff-like (SVK) orthotropic isochoric strain energy part, (e) Saint-Venant-Kirchhoff-like non-isochoric orthotropic strain energy part, (f) Mixed model (d) and (e), (g) Homogenized model with SVK-like fibers, and (h) Homogenized model with Almansi fibers.

Organizing the proposed models in the above mentioned unique algebraic (polynomial) representation one shows that the elastic constants of the proposed models are easily related to usual linear elastic experimental tests. Is opens the possibility of using well established linear experimental tests to find initial ground constants of large deformable materials. A tailoring fiber-reinforced solid model - in which discrete fibers are immersed into continuous matrix – is also presented and used to generate ground elastic constants for numerical tests. The proposed models are implemented in an in-house FEM code and comparisons among their mechanical behavior give clues to their behavior and opens possibilities for future implementations. Finally, model (g) is selected to successfully simulate the pig myocardium tissue experimentally tested by Dokos et al. (2002) and numerically modeled by Holzapfel and Ogden (2009). In appendix A a list of symbols and abbreviations is provided to simplify the reading.

2 GENERAL STRAIN ENERGY FUNCTION AND FLORY' DECOMPOSITION

In this section the adopted notation, as well as basic information necessary to the proposed developments are provided. As described by Holzapfel (2000), one assumes that the specific strain energy $W(\mathbf{C})$ is a function of the Right-Cauchy-Green stretch tensor $\mathbf{C} = \mathbf{A}^T \cdot \mathbf{A}$ (in which $\mathbf{A}$ is the deformation gradient) and respects the growth condition given by:

$$\lim_{J \to +\infty} W = +\infty$$

and

$$\lim_{J \to 0^+} W = +\infty \tag{1}$$

in which $J^2 = Det(\mathbf{C})$.

The normalization condition - when the strain energy function has a minimum value - is also adopted, i.e.:

$$W(\mathbf{C} = \mathbf{I}) = W(\mathbf{E} = \mathbf{0}) = 0 \tag{2}$$

in which $\mathbf{E} = (\mathbf{C} - \mathbf{I})/2$ is the Green-Lagrange strain and $\mathbf{I}$ is the identity tensor of second order. Finally the proposed strain energy functions increase with strain, i.e., according to Eq. (2) $W \geq 0$.

Following Flory (1961), one writes the isochoric part of $\mathbf{A}$ as

$$\overline{\mathbf{A}} = J^{-1/3}\mathbf{A}$$

With

$$Det\left(\overline{\mathbf{A}}\right) = Det\left(\mathbf{A}\right)\left(J^{-1/3}\right)^3 = 1 \tag{3}$$

and the volumetric part of $\mathbf{A}$ as

$$\hat{\mathbf{A}} = J^{1/3}\mathbf{I}$$

$$Det\left(\hat{\mathbf{A}}\right) = Det\left(\mathbf{I}\right)\left(J^{1/3}\right)^3 = J \tag{4}$$

Thus, one recovers the deformation gradient by the product

$$\mathbf{A} = \hat{\mathbf{A}} \cdot \overline{\mathbf{A}} = \overline{\mathbf{A}} \cdot \hat{\mathbf{A}} \tag{5}$$

Applying this definition to the Cauchy-Green stretch one writes

$$\overline{\mathbf{C}} = \overline{\mathbf{A}}^T \cdot \overline{\mathbf{A}} = J^{-2/3}\mathbf{C} \tag{6}$$

$$\hat{\mathbf{C}} = \hat{\mathbf{A}}^T \cdot \hat{\mathbf{A}} = J^{2/3}\mathbf{I} \tag{7}$$

$$\mathbf{C} = \hat{\mathbf{C}} \cdot \overline{\mathbf{C}} = \overline{\mathbf{C}} \cdot \hat{\mathbf{C}} \tag{8}$$

$$Det\left(\overline{\mathbf{C}}\right) = \left(J^{-2/3}\right)^3 J^2 = 1$$

$$Det\left(\hat{\mathbf{C}}\right) = \left(J^{2/3}\right)^3 = J^2 \tag{9}$$

Thus, $\overline{\mathbf{C}}$ is the isochoric part of the Cauchy-Green stretch and $\hat{\mathbf{C}}$ is its volumetric part. From this decomposition the strain energy can be written as a sum of volumetric and isochoric parts, as follows:

$$W = \hat{W}(\hat{\mathbf{C}}) + \overline{W}(\overline{\mathbf{C}}) = \hat{W}(J) + \overline{W}(\overline{\mathbf{C}})$$

or

$$W = \hat{W}(J) + \overline{W}(\overline{\mathbf{E}}) \tag{10}$$

in which the isochoric-like Green-Lagrange strain is defined as:

$$\overline{\mathbf{E}} = J^{-2/3}\mathbf{E} = \frac{1}{2}(J^{-2/3}\mathbf{C} - J^{-2/3}\mathbf{I}) = \frac{1}{2}(\overline{\mathbf{C}} - \overline{\mathbf{I}}) \tag{11}$$

Without loss of generality, for all models the volumetric part of the strain energy proposed by Hartmann and Neff (2003) is adopted, i.e.:

$$\hat{W}(J)=\frac{K}{8n^2}\left(J^{2n}+J^{-2n}-2\right) \tag{12}$$

In which n is an arbitrary constant that can be used to calibrate the large strain behavior of models and K is the bulk modulus that can measured at the small strain as described in Eq. (16). Deriving Eq. (12) regarding the Green strain, one finds the volumetric part of the Second Piola-Kirchhoff stress as:

$$\hat{S}_{ij}=\frac{\partial\hat{W}}{\partial E_{ij}}=\frac{K}{4n}\left(J^{2n}-J^{-2n}\right)D_{ij} \tag{13}$$

in which $\mathbf{D}=\mathbf{C}^{-1}$ and indices indicates Cartesian coordinates that will be extended to orthotropic directions in section 3. The second derivative of $\hat{W}$ regarding the Green strain results the volumetric part of the tangent constitutive stiffness tensor $\hat{\mathfrak{H}}$ given by:

$$\hat{\mathfrak{H}}_{ijk\ell}=\frac{\partial^2\hat{W}}{\partial E_{ij}\partial E_{k\ell}}=\frac{K}{4n}\left\{2n\left(J^{2n}+J^{-2n}\right)D_{ij}D_{k\ell}+\left(J^{2n}-J^{-2n}\right)\left(D_{ij}D_{k\ell}-2D_{ik}D_{j\ell}\right)\right\} \tag{14}$$

Making the limit of Eq. (14) for $\mathbf{E}\to\mathbf{0}$ one finds:

$$\hat{\mathfrak{H}}^0_{ijk\ell}=\lim_{\substack{E\to 0\\ J\to 1}}\hat{\mathfrak{H}}_{ijk\ell}=K\delta_{ij}\delta_{k\ell} \tag{15}$$

Considering the complete elastic tensor $\mathfrak{H}^0$ for small strains (experimentally determined) one can achieve the bulk modulus by the well known relation:

$$K=\left(\mathfrak{H}^0_{iijj}/9\right) \tag{16}$$

thus, the bulk modulus used in the Hartmann – Neff portion of large strain constitutive models can be determined at small strain experiments.

The isochoric portion of the orthotropic models to be proposed is generically written as $\overline{W}(\overline{\mathbf{C}})$ or $\overline{W}(\overline{\mathbf{E}})$. Making the first derivative of this strain energy portion regarding the Green-Lagrange strain, results:

$$\overline{S}_{ij}=\frac{\partial\overline{W}}{\partial E_{ij}}=\frac{\partial}{\partial E_{ij}}\left(J^{-4/3}W^*\right)=-\frac{4}{3}J^{-4/3}D_{ij}W^*(\mathbf{E})+J^{-4/3}\frac{\partial W^*(\mathbf{E})}{\partial E_{ij}} \tag{17}$$

in which, using Eq. (11), $\overline{W}=J^{-4/3}W^*$, W^* is a usual strain energy function without imposing isochoric behavior and $\overline{\mathbf{S}}$ is the deviatory part of the second Piola-Kirchhoff stress. The second derivative of $\overline{W}$ regarding the Green strain results the isochoric part of the tangent constitutive stiffness tensor $\overline{\mathfrak{H}}$ given by:

$$\overline{\mathfrak{H}}_{ijk\ell}=\frac{\partial^2\overline{W}}{\partial E_{ij}\partial E_{k\ell}}=J^{-4/3}\left\{\frac{8}{9}\left[2D_{k\ell}D_{ij}+3D_{ik}D_{\ell j}\right]W^*(\mathbf{E})-\frac{4}{3}\left[D_{ij}\frac{\partial W^*(\mathbf{E})}{\partial E_{k\ell}}+D_{k\ell}\frac{\partial W^*(\mathbf{E})}{\partial E_{ij}}\right]+\frac{\partial^2 W^*(\mathbf{E})}{\partial E_{ij}\partial E_{k\ell}}\right\} \tag{18}$$

In order to find relations of large strain elastic constants and small strains counterparts, the limit for $\mathbf{E}\to\mathbf{0}$ of Eq. (18) is performed after defining the specific isochoric strain energy functions.

3 CLASSICAL ORTHOTROPIC INVARIANTS AND SIMPLIFIED NOTATION

Seeking to clarify the understanding of classical orthotropic invariants of the Cauchy-Green stretching tensor, one presents a geometric interpretation regarding the orthotropic vectors associated with the orthotropic planes. In Fig. 1 the unit vector $\vec{o}^{\,i}$ indicates a general orthotropic direction i (fiber alignment) which means that any rotation around this axis does not change the elastic properties of the continuum. In Fig. 1 and along this paper the following notation will be used:

$$Z_{ij} = \vec{o}^{\,i} \cdot \mathbf{Z} \cdot \vec{o}^{\,j} \tag{19}$$

which means that the components of tensors are given regarding the orthotropic axes.

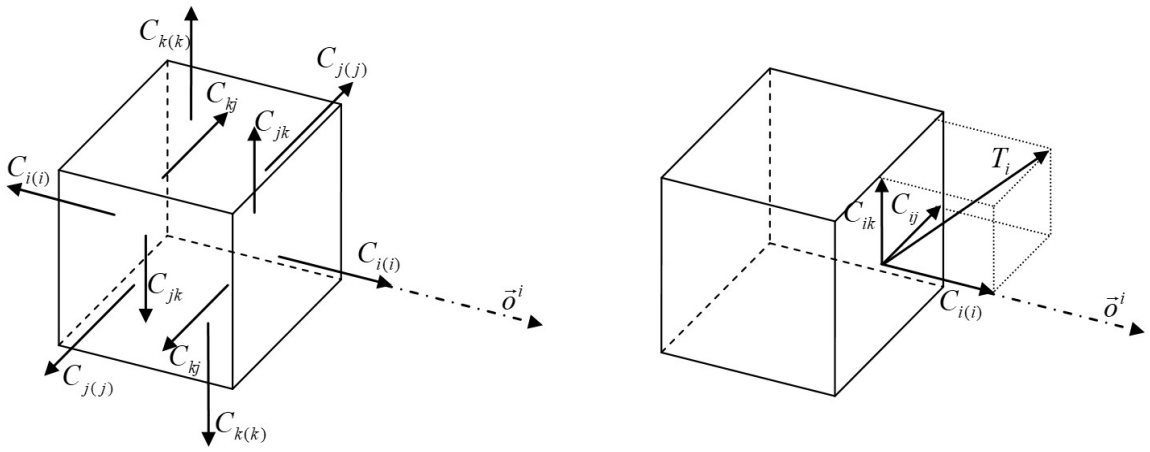

(a) First set of invariants *(b) Second set of invariants*

Figure1 Orthotropic invariant tips for direction (i).

In order to understand Fig. 1, one should imagine arrows as components of the Cauchy-Stretch tensor, in a similar way one understands the Cauchy stress representation. Making this analogy, from Fig. 1(a), one identifies the following 9 orthotropic invariants (first set), i.e., not sensible to rotation around a general axis $i = 1,2,3$:

$$C_{i(i)},\ Tr\begin{bmatrix} C_{j(j)} & C_{jk} \\ C_{kj} & C_{k(k)} \end{bmatrix} \text{ and } Det\begin{bmatrix} C_{j(j)} & C_{jk} \\ C_{kj} & C_{k(k)} \end{bmatrix} \tag{20}$$

and from Fig. 1(b) one identifies the following 3 invariants (second set) also independent of rotation around axis $i = 1,2,3$:

$$T_{ijk}^2 = C_{i(i)}^2 + C_{ij}^2 + C_{ik}^2$$

with

$$i, j, k \tag{21}$$

in cyclic permutation observing that $C_{ij} = C_{ji}$.

The well known 3 isotropic invariants, that are not sensible to any rotation, are written as:

$$Tr\,\mathbf{C},\ Tr\,\mathbf{C}^2 \text{ and } Tr\,\mathbf{C}^3 \tag{22}$$

or, equivalently, as Spencer (1984) shows, the isotropic invariants may be written as:

$$I_1 = Tr\,\mathbf{C}\,,\ I_2 = Tr\left(Adj\,\mathbf{C}\right) \text{ and } I_3 = Det\,\mathbf{C} = J^2 \tag{23}$$

Considering that the Flory's decomposition allows separating the volumetric and isochoric parts of the strain energy function, one chooses to write the 15 invariants (9 from Fig. 1(a), 3 from Fig. 1(b) and 3 isotropic) detaching the volumetric part as follows:

$$\overline{I}_1 = Tr\,\overline{\mathbf{C}}\,,\ \overline{I}_2 = Tr\left(Adj\,\overline{\mathbf{C}}\right),\ J^2 = I_3 = \hat{I}_3 = Det\,\hat{\mathbf{C}}\,, \tag{24}$$

$$\overline{C}_{i(i)}\,,\ Tr\begin{bmatrix}\overline{C}_{j(j)} & \overline{C}_{jk}\\ \overline{C}_{kj} & \overline{C}_{k(k)}\end{bmatrix},\ Det\begin{bmatrix}\overline{C}_{j(j)} & \overline{C}_{jk}\\ \overline{C}_{kj} & \overline{C}_{k(k)}\end{bmatrix},\ \overline{T}^2_{ijk} = \overline{C}^2_{i(i)} + \overline{C}^2_{ij} + \overline{C}^2_{ik} \tag{25}$$

As will be seen in next section, it is not necessary to use all these fifteen invariants (Holzapfel and Ogden, 2010) with a volumetric control (growth condition) (Hartmann and Neff, 2003) to assemble a complete isochoric positive polynomial. Moreover, the minimum parameter strain energy function (Rubin, 2016; Shariff, 2013; Spencer, 1984; Aguiar and Lopes da Rocha, 2018; Holzapfel and Ogden, 2010) adopted here uses the equivalent invariants defined by Eq. (24) plus

$$\overline{I}_4 = \overline{C}_{11}\,,\ \overline{I}_5 = \overline{C}^2_{11}\,,\ \overline{I}_6 = \overline{C}_{22}\,, \text{ and } \overline{I}_7 = \overline{C}^2_{22} \tag{26}$$

,i.e., 7 invariants. One should note that the four invariants of Eq. (26) are a subset of the twelve invariants of Eq (25).

4 STUDIED STRAIN ENERGY FUNCTIONS

The easier way to clarify the equivalence of various fundamental models (using or not the usual Right-Cauchy-Green stretch tensor orthotropic invariants) is to show that all energy functions studied here can be written in the following unified form:

$$\begin{aligned} W = {} & \frac{K}{8n^2}\left(J^{2n} + J^{-2n} - 2\right) + J^{-4/3}\left\{\left[a_1 C_{11} + a_2 C_{22} + a_3 C_{33}\right] + \right.\\ & + \left[a_4\left(C_{22}C_{33}\right) + a_5\left(C_{11}C_{33}\right) + a_6\left(C_{11}C_{22}\right)\right] + a_7 C^2_{23} + \\ & \left. + a_8 C^2_{13} + a_9 C^2_{12} + a_{10} C^2_{11} + a_{11} C^2_{22} + a_{12} C^2_{33} + \overline{R}\right\} \end{aligned} \tag{27}$$

in which a_1, a_2, a_3 and $\overline{R}$ guaranty the normality condition and zero stress at zero strain, i.e., are not proper elastic constants. The bulk modulus K can be dependent of the other elastic constants (see Eq. (16)) if linear experiments are used to define elastic ground constants, but also can be defined as an independent constant if this relation is not considered for large strain models. Thus, the total number of elastic coefficients in Eq. (27) (independent or not) may be considered 10, (including K) or 9, i.e., a_4 through a_{12}. The differences among models are regarded to the computation of coefficients a_i and constant $\overline{R}$, that makes easy or difficult the material characterization.

4.1 Model (a): Minimum classical orthotropic invariants strain energy function

The minimum parameter energy function (Rubin, 2016; Shariff, 2013; Spencer, 1984; Aguiar and Lopes da Rocha, 2018; Holzapfel and Ogden, 2010) use invariants defined by Eqs. (24) and (26), remembering that $\overline{C}^2_{ij} = J^{-4/3}C^2_{ij}$. After some tedious algebraic manipulation (Spencer, 1984), one has:

$$
\begin{aligned}
W = {} & \bar{m}_3\left(J^{2n}+J^{-2n}-2\right)+J^{-4/3}\left\{\bar{m}_1\left(C_{11}+C_{22}+C_{33}-3\right)^2+\right. \\
& +\bar{m}_2\left[Det\begin{bmatrix}C_{22} & C_{23}\\ C_{32} & C_{33}\end{bmatrix}-1+Det\begin{bmatrix}C_{11} & C_{13}\\ C_{31} & C_{33}\end{bmatrix}-1+Det\begin{bmatrix}C_{11} & C_{12}\\ C_{21} & C_{22}\end{bmatrix}-1\right]+ \\
& \left.+\bar{m}_4(C_{11}-1)^2+\bar{m}_5\left(C_{11}^2+C_{12}^2+C_{13}^2-1\right)+\bar{m}_6(C_{22}-1)^2+\bar{m}_7\left(C_{22}^2+C_{12}^2+C_{23}^2-1\right)\right\}
\end{aligned}
\tag{28}
$$

in which $\bar{m}_i$ can be defined as the elastic constants - energy conjugate - to the chosen invariants. One needs to subtract the unity from each $C_{i(i)}$ in order to guaranty the normality condition, which is similar to write the energy function using the Green-Lagrange strain.

After simple algebraic manipulations, Eq. (28) is rewritten exactly as Eq. (27) with:

$$
\begin{aligned}
& a_1=-(6\bar{m}_1+2\bar{m}_4),\ a_2=-(6\bar{m}_1+2\bar{m}_6),\ a_3=-6\bar{m}_1, \\
& a_4=\left(\bar{m}_2+2\bar{m}_1\right),\ a_5=\left(\bar{m}_2+2\bar{m}_1\right),\ a_6=\left(\bar{m}_2+2\bar{m}_1\right), \\
& a_7=\left(\bar{m}_7-\bar{m}_2\right),\ a_8=\left(\bar{m}_5-\bar{m}_2\right),\ a_9=\left(\bar{m}_5+\bar{m}_7-\bar{m}_2\right), \\
& a_{10}=(\bar{m}_1+\bar{m}_4+\bar{m}_5),\ a_{11}=(\bar{m}_1+\bar{m}_6+\bar{m}_7),\ a_{12}=\bar{m}_1 \\
& \bar{R}=(9\bar{m}_1-3\bar{m}_2+\bar{m}_4+\bar{m}_6-\bar{m}_5-\bar{m}_7)
\end{aligned}
\tag{29}
$$

recalling that a_1, a_2, a_3 and $\bar{R}$ only guarantee the normality condition and zero stress at zero strain.

The equality $a_4=a_5=a_6$ means that some elements of the linear elastic constitutive tensor (when $\mathbf{C}\to\mathbf{I}$), see Eqs. (27) and (A12), are equal to each other, i.e., $\mathfrak{H}_{1122}=\mathfrak{H}_{1133}=\mathfrak{H}_{2233}$, limiting the independence of the orthotropic parameters at the small strain range. It is clear that the minimum parameters strain energy function is a theoretical potential not able to model general materials, even at small strain range.

It is important to mention that in this classical and fundamental representation, references (Rubin, 2016; Shariff, 2013; Spencer, 1984; Aguiar and Lopes da Rocha, 2018) do not consider the bulk modulus as a dependent elastic constant achieved at small strains (as they are not interested in small strains at all) thus the number of independent parameters is 7. However, if one thinks it is adequate to use Eq. (16) to define the bulk modulus for a specific material at small strains, the number of parameters to be experimentally achieved reduces to 6. It is interesting to mention that the characterization of materials using the formalism of expression (27) may be difficult, but model (d), given in section 4.4, indicates a simpler characterization strategy, at linear range.

4.2 Model (b): Nine parameters strain energy based on classical orthotropic invariants

As hyperelastic models may have more parameters in order to better reproduce material behavior, in this case all 15 invariants defined in Eqs. (24) and (25) are used. and the resulting elastic constants at the formalism of Eq. (27) is investigated. Stating from the 15 invariants and adopting general elastic constants for each one, one writes the strain energy as:

$$
\begin{aligned}
W = {} & \frac{K}{8n^2}\left(J^{2n}+J^{-2n}-2\right)+J^{-4/3}\Big\{\ k_1^{iso}\left[\left(C_{11}+C_{22}+C_{33}-3\right)^2\right]+ \\
& +k_2^{iso}\left[Det\begin{bmatrix}C_{22} & C_{23}\\ C_{32} & C_{33}\end{bmatrix}-1+Det\begin{bmatrix}C_{11} & C_{13}\\ C_{31} & C_{33}\end{bmatrix}-1+Det\begin{bmatrix}C_{11} & C_{12}\\ C_{21} & C_{22}\end{bmatrix}-1\right]+ \\
& +k_1\left(C_{11}-1\right)^2+k_2\left(C_{22}-1\right)^2+k_3\left(C_{33}-1\right)^2+ \\
& +k_4\left(Det\begin{bmatrix}C_{22} & C_{23}\\ C_{32} & C_{33}\end{bmatrix}-1\right)+k_5\left(Det\begin{bmatrix}C_{11} & C_{13}\\ C_{31} & C_{33}\end{bmatrix}-1\right)+k_6\left(Det\begin{bmatrix}C_{11} & C_{12}\\ C_{21} & C_{22}\end{bmatrix}-1\right)+ \\
& +k_7\left(C_{33}+C_{22}-2\right)^2+k_8\left(C_{11}+C_{33}-2\right)^2+k_9\left(C_{11}+C_{22}-2\right)+ \\
& +k_{10}\left(C_{11}^2+C_{12}^2+C_{13}^2-1\right)+k_{11}\left(C_{22}^2+C_{12}^2+C_{23}^2-1\right)+k_{12}\left(C_{33}^2+C_{13}^2+C_{23}^2-1\right)\Big\}
\end{aligned}
\tag{30}
$$

in which superscript iso means isotropic terms and $k_3^{iso}=K/(8n^2)$.

After some tedious algebraicmanipulations one writes Eq. (30) exactly as Eq. (27) with the following constants correspondences:

$$
\begin{aligned}
& a_1=(-2k_1-4k_8-4k_9-6k_1^{iso}),\ a_2=(-2k_2-4k_7-4k_9-6k_1^{iso}),\ a_3=(-2k_3-4k_7-4k_8-6k_1^{iso}), \\
& a_4=(2k_7+k_4+k_2^{iso}+2k_1^{iso}),\ a_5=(2k_8+k_5+k_2^{iso}+2k_1^{iso}),\ a_6=(2k_9+k_6+k_2^{iso}+2k_1^{iso}), \\
& a_7=(k_{11}+k_{12}-k_4-k_2^{iso}),\ a_8=(k_{10}+k_{12}-k_5-k_2^{iso}),\ a_9=(k_{10}+k_{11}-k_6-k_2^{iso}), \\
& a_{10}=(k_8+k_9+k_{10}+k_1^{iso}),\ a_{11}=(k_7+k_9+k_{11}+k_1^{iso}),\ a_{12}=(k_7+k_8+k_{10}+k_1^{iso}) \\
& \overline{R}=(9k_1^{iso}-3k_2^{iso}+k_1+k_2+k_3+4k_7+4k_8+4k_9-k_4-k_5-k_6-k_{10}-k_{11}-k_{12})
\end{aligned}
\tag{31}
$$

In this case (like linear elasticity) from the starting 15 elastic constants, one has 9 independent ones a_4 trough a_{12}. The bulk modulus is then calculated from the other parameters at small strains, see Eq. (16) and recall that a_1, a_2, a_3 and $\overline{R}$ only guarantee the normality condition and zero stress at zero strain.

4.3 Model (c): Hyperelastic extension of the linear constitutive model written as Spencer (1984)

In this item, the linear constitutive model is written in the format proposed by Spencer (1984) and, knowing that the Green-Lagrange strain approaches the linear strain when it is small, the linear strains are replaced by the isochoric Green strain defined in Eq. (11). In addition, the same volumetric portion of the previous models is added in order to guaranty the growth condition, not guaranteed by linear elasticity. This procedure is reproduced in the following expression:

$$
\begin{aligned}
W = {} & \frac{K}{8n^2}\left(J^{2n}+J^{-2n}-2\right)+J^{-4/3}\left\{\frac{\lambda}{2}\left(E_{11}+E_{22}+E_{33}\right)^2+\mu\left(E_{11}^2+E_{22}^2+E_{33}^2+2E_{12}^2+2E_{13}^2+2E_{23}^2\right)+\right. \\
& +\left(\alpha_1E_{11}+\alpha_2E_{22}\right)\left(E_{11}+E_{22}+E_{33}\right)+2\mu_1\left(E_{11}^2+E_{12}^2+E_{13}^2\right)+2\mu_2\left(E_{22}^2+E_{12}^2+E_{23}^2\right)+ \\
& \left.+\frac{1}{2}\beta_1E_{11}^2+\frac{1}{2}\beta_2E_{22}^2+\beta_3E_{11}E_{22}\right\}
\end{aligned}
\tag{32}
$$

in which λ, μ, α_1, α_2, μ_1, μ_2, β_1, β_2 end β_3 are Spencer's elastic constants.

After some algebraic manipulations one achieves the unified representation of Eq. (27), with the following elastic constants correspondences:

$$
\begin{aligned}
&a_1 = (-\alpha_1 - \alpha_2 - 3\lambda - 3\alpha_1),\ a_2 = (-\alpha_1 - \alpha_2 - 3\lambda - 3\alpha_2),\ a_3 = (-\alpha_1 - \alpha_2 - 3\lambda)\\
&a_4 = (\alpha_2 + \lambda),\ a_5 = (\alpha_1 + \lambda),\ a_6 = (\alpha_1 + \alpha_2 + \lambda + \beta_3),\ a_7 = (2\mu + 2\mu_2)\\
&a_8 = (2\mu + 2\mu_1),\ a_9 = (2\mu + 2\mu_1 + 2\mu_2),\ a_{10} = \left(\lambda/2 + \mu + \alpha_1 + 2\mu_1 + \beta_1/2\right)\\
&a_{11} = \left(\lambda/2 + \mu + \alpha_2 + 2\mu_2 + \beta_2/2\right),\ a_{12} = \left(\lambda/2 + \mu\right)\\
&\overline{R} + \left(9\lambda/2 + 3\alpha_1 + 3\alpha_2 - \beta_1/2 - \beta_2/2 - \beta_3 - 2\mu_2 - 2\mu_1 - 3\mu\right)
\end{aligned}
\tag{33}
$$

Again, one has 9 independent elastic constants a_4 trough a_{12} considering the bulk modulus calculated from the other parameters at small strains as in linear elasticity.

As a conclusion of the above developments, despite the formalism adopted to write the strain energy from classical orthotropic invariants, after algebraic operations, one will achieve Eq. (27) that has components (in the orthotropic directions) of the Green-stretch tensor as main variables.

4.4 Model (d): Saint-Venant-Kirchhoff-like orthotropic isochoric strain energy part

Observing that model (c) is an extension of Spencer's linear orthotropic constitutive law with 9 elastic constants (being K not a free elastic constant in this case) a direct association (not found in literature) will be made here with the generalized linear orthotropic Hooke's law (Lekhnitskii, 1963) that also has 9 well defined elastic constants. From this Hooke's law the Saint-Venant-Kirchhoff-like (SVK-like) orthotropic constitutive equation is written substituting linear strains by Green-Lagrange strains (equal to each other at small strains), see appendix B.

From the orthotropic SVK-like expressions described in the appendix and including the Flory's decomposition, from Eqs. (10), (15) and (18), one finds in a limiting process for $\mathbf{E} \to \mathbf{0}$ that the total linear elastic constitutive tensor $\mathcal{H}^0_{ijk\ell}$ can be written as:

$$\mathcal{H}^0_{ijk\ell} = \hat{\mathcal{H}}^0_{ijk\ell} + \overline{\mathcal{H}}^0_{ijk\ell}$$

or

$$\overline{\mathcal{H}}^0_{ijk\ell} = \mathcal{H}^0_{ijk\ell} - K\delta_{ij}\delta_{k\ell} \tag{34}$$

in which $\hat{\mathcal{H}}^0_{ijk\ell}$ is the volumetric part of the tangent constitutive elastic tensor at small strains, see equation (15), $\mathcal{H}^0_{ijk\ell}$ is the full linear constitutive tensor and $\overline{\mathcal{H}}^0_{ijk\ell}$ is the isochoric part of the linear constitutive tensor.

As $\mathcal{H}^0_{ijk\ell}$ is easily achieved by the inversion of the linear compliance tensor (see appendix B), the basic elastic constants for finite strain models can be achieved by well known experimental tests for small strain elasticity. In particular, the model proposed in this item is also related to the unified Eq. (27) facilitating this interpretation and making this procedure a simple task. Thus, the isochoric specific strain energy part of the proposed orthotropic model is simply written as:

$$\overline{W}(\overline{E}) = \frac{1}{2}\overline{E}_{ij}\overline{\mathcal{H}}^0_{ijk\ell}\overline{E}_{k\ell} \tag{35}$$

see Eq. (11). After some algebraic manipulations one writes the strain energy in the unified format of Eq. (27), as:

$$
\begin{aligned}
&W = \frac{K}{8n^2}\left(J^{2n} + J^{-2n} - 2\right) + \\
&+\frac{J^{-4/3}}{8}\Big\{-2\Big[(\bar{\mathcal{H}}^0_{1111} + \bar{\mathcal{H}}^0_{1122} + \bar{\mathcal{H}}^0_{1133})C_{11} + (\bar{\mathcal{H}}^0_{2222} + \bar{\mathcal{H}}^0_{1122} + \bar{\mathcal{H}}^0_{2233})C_{22} + (\bar{\mathcal{H}}^0_{3333} + \bar{\mathcal{H}}^0_{1133} + \bar{\mathcal{H}}^0_{2233})C_{33}\Big] + \\
&+2\bar{\mathcal{H}}^0_{2233}C_{22}C_{33} + 2\bar{\mathcal{H}}^0_{1133}C_{11}C_{33} + 2\bar{\mathcal{H}}^0_{1122}C_{11}C_{22} + 2(\bar{\mathcal{H}}^0_{2323}C^2_{23} + \bar{\mathcal{H}}^0_{1313}C^2_{13} + \bar{\mathcal{H}}^0_{1212}C^2_{12}) + \\
&+(\bar{\mathcal{H}}^0_{1111}C^2_{11} + \bar{\mathcal{H}}^0_{2222}C^2_{22} + \bar{\mathcal{H}}^0_{3333}C^2_{33}) + \\
&+(\bar{\mathcal{H}}^0_{1111} + \bar{\mathcal{H}}^0_{2222} + \bar{\mathcal{H}}^0_{3333} + 2\bar{\mathcal{H}}^0_{1122} + 2\bar{\mathcal{H}}^0_{1133} + 2\bar{\mathcal{H}}^0_{2233})\Big\}
\end{aligned}
\tag{36}
$$

And the correspondence of elastic constants is simply:

$$
\begin{aligned}
&a_1 = -\frac{1}{4}(\bar{\mathcal{H}}^0_{1111} + \bar{\mathcal{H}}^0_{1122} + \bar{\mathcal{H}}^0_{1133}), a_2 = -\frac{1}{4}(\bar{\mathcal{H}}^0_{2222} + \bar{\mathcal{H}}^0_{1122} + \bar{\mathcal{H}}^0_{2233}), a_3 = -\frac{1}{4}(\bar{\mathcal{H}}^0_{3333} + \bar{\mathcal{H}}^0_{1133} + \bar{\mathcal{H}}^0_{2233}) \\
&a_4 = \frac{1}{4}\bar{\mathcal{H}}^0_{2233},\ a_5 = \frac{1}{4}\bar{\mathcal{H}}^0_{1133},\ a_6 = \frac{1}{4}\bar{\mathcal{H}}^0_{1122}, \\
&a_7 = \frac{1}{4}\bar{\mathcal{H}}^0_{2323},\ a_8 = \frac{1}{4}\bar{\mathcal{H}}^0_{1313},\ a_9 = \frac{1}{4}\bar{\mathcal{H}}^0_{1212}, \\
&a_{10} = \frac{1}{8}\bar{\mathcal{H}}^0_{1111}, a_{11} = \frac{1}{8}\bar{\mathcal{H}}^0_{2222},\ a_{12} = \frac{1}{8}\bar{\mathcal{H}}^0_{3333} \\
&\bar{R} = \frac{1}{8}(\bar{\mathcal{H}}^0_{1111} + \bar{\mathcal{H}}^0_{2222} + \bar{\mathcal{H}}^0_{3333} + 2\bar{\mathcal{H}}^0_{1122} + 2\bar{\mathcal{H}}^0_{1133} + 2\bar{\mathcal{H}}^0_{2233})\Big\}
\end{aligned}
\tag{37}
$$

i.e., in this case the general elastic coefficients (a_4 through a_{12}) of Eq. (27) have a direct correspondence with simple linear elastic experiments and can be identified in the linear stiffness constitutive tensor using Eqs. (34), (15) and (18), written in Voigt's notation, as:

$$
\bar{\mathcal{H}}^0 = \begin{bmatrix}
\bar{\mathcal{H}}^0_{1111} & \bar{\mathcal{H}}^0_{1122} & \bar{\mathcal{H}}^0_{1133} & 0 & 0 & 0 \\
 & \bar{\mathcal{H}}^0_{2222} & \bar{\mathcal{H}}^0_{2233} & 0 & 0 & 0 \\
 & & \bar{\mathcal{H}}^0_{3333} & 0 & 0 & 0 \\
 & & & 2\bar{\mathcal{H}}^0_{2323} & 0 & 0 \\
 & Sym & & & 2\bar{\mathcal{H}}^0_{1313} & 0 \\
 & & & & & 2\bar{\mathcal{H}}^0_{1212}
\end{bmatrix} = \begin{bmatrix}
a_{10} & a_6 & a_5 & 0 & 0 & 0 \\
 & a_{11} & a_4 & 0 & 0 & 0 \\
 & & a_{11} & 0 & 0 & 0 \\
 & & & 2a_7 & 0 & 0 \\
 & Sym & & & 2a_8 & 0 \\
 & & & & & 2a_9
\end{bmatrix}
\tag{38}
$$

4.5 Model (e): Saint-Venant-Kirchhoff-like non-isochoric orthotropic strain energy part

In order to show simple modifications that one can introduce in constitutive models, changing the material response at large strains, a simple model that doesn't use the Flory's decomposition for strains at the isochoric SVK-like part of the model is presented. This model applies Eq. (34) in order to keep, at small strains, the volumetric control only in the first part of the strain energy function (volumetric part), resulting:

$$
\begin{aligned}
&W = \frac{K}{8n^2}\left(J^{2n} + J^{-2n} - 2\right) + \\
&+\frac{1}{8}\Big\{-2\Big[(\bar{\mathcal{H}}^0_{1111} + \bar{\mathcal{H}}^0_{1122} + \bar{\mathcal{H}}^0_{1133})C_{11} + (\bar{\mathcal{H}}^0_{2222} + \bar{\mathcal{H}}^0_{1122} + \bar{\mathcal{H}}^0_{2233})C_{22} + (\bar{\mathcal{H}}^0_{3333} + \bar{\mathcal{H}}^0_{1133} + \bar{\mathcal{H}}^0_{2233})C_{33}\Big] + \\
&+2\bar{\mathcal{H}}^0_{2233}C_{22}C_{33} + 2\bar{\mathcal{H}}^0_{1133}C_{11}C_{33} + 2\bar{\mathcal{H}}^0_{1122}C_{11}C_{22} + 2(\bar{\mathcal{H}}^0_{2323}C^2_{23} + \bar{\mathcal{H}}^0_{1313}C^2_{13} + \bar{\mathcal{H}}^0_{1212}C^2_{12}) + \\
&+(\bar{\mathcal{H}}^0_{1111}C^2_{11} + \bar{\mathcal{H}}^0_{2222}C^2_{22} + \bar{\mathcal{H}}^0_{3333}C^2_{33}) + \\
&+(\bar{\mathcal{H}}^0_{1111} + \bar{\mathcal{H}}^0_{2222} + \bar{\mathcal{H}}^0_{3333} + 2\bar{\mathcal{H}}^0_{1122} + 2\bar{\mathcal{H}}^0_{1133} + 2\bar{\mathcal{H}}^0_{2233})\Big\}
\end{aligned}
\tag{39}
$$

see the absence of $J^{-4/3}$ at the second part of the model when compared with Eq. (36) meaning that $\mathbf{E}$ is used instead of $\bar{\mathbf{E}}$.

At small strain range ($J \cong 1$), the same correspondence with Eq. (34) described by Eq. (38) is achieved, revealing that the difference between models (d) and (e) occurs at large strains. For isochoric situations models (d) and (e) will have the same behavior.

4.6 Model (f): Mixed model (d) and (e)

Like the proposed model (e), this model doesn't use the Flory's decomposition at the SVK-like part of the model; however, it split the volumetric control at small strains for both parts of the model, using the following equations, instead of Eqs. (34) and (39):

$$
\tilde{\mathcal{H}}^0_{ijk\ell} = \mathcal{H}^0_{ijk\ell} - \beta K \delta_{ij}\delta_{k\ell}
\tag{40}
$$

$$
\begin{aligned}
&W = \beta\frac{K}{8n^2}\left(J^{2n} + J^{-2n} - 2\right) + \\
&+\frac{1}{8}\Big\{-2\Big[(\tilde{\mathcal{H}}^0_{1111} + \tilde{\mathcal{H}}^0_{1122} + \tilde{\mathcal{H}}^0_{1133})C_{11} + (\tilde{\mathcal{H}}^0_{2222} + \tilde{\mathcal{H}}^0_{1122} + \tilde{\mathcal{H}}^0_{2233})C_{22} + (\tilde{\mathcal{H}}^0_{3333} + \tilde{\mathcal{H}}^0_{1133} + \tilde{\mathcal{H}}^0_{2233})C_{33}\Big] + \\
&+2\tilde{\mathcal{H}}^0_{2233}C_{22}C_{33} + 2\tilde{\mathcal{H}}^0_{1133}C_{11}C_{33} + 2\tilde{\mathcal{H}}^0_{1122}C_{11}C_{22} + 2(\tilde{\mathcal{H}}^0_{2323}C^2_{23} + \tilde{\mathcal{H}}^0_{1313}C^2_{13} + \tilde{\mathcal{H}}^0_{1212}C^2_{12}) + \\
&+(\tilde{\mathcal{H}}^0_{1111}C^2_{11} + \tilde{\mathcal{H}}^0_{2222}C^2_{22} + \tilde{\mathcal{H}}^0_{3333}C^2_{33}) + \\
&+(\tilde{\mathcal{H}}^0_{1111} + \tilde{\mathcal{H}}^0_{2222} + \tilde{\mathcal{H}}^0_{3333} + 2\tilde{\mathcal{H}}^0_{1122} + 2\tilde{\mathcal{H}}^0_{1133} + 2\tilde{\mathcal{H}}^0_{2233})\Big\}
\end{aligned}
\tag{41}
$$

in which $0 \le \beta \le 1$. For $\beta = 0$ the model falls in the pure SVK-like model for orthotropic materials (violating the growth condition) and for $\beta = 1$ the model falls in model (e). In examples $\beta = 1/2$ is adopted to illustrate the general behavior of this model. It is not necessary to show that Eq. (41) can also be written as Eq. (27).

4.7 Model (g): Homogenized model with SVK-like fibers

The transition from Eq. (35) to Eq. (36) in model (d) involves only the relationship (11). The transition from model (d) to model (e) is just the replacement, in Eq. (35), of equation (11) by the standard format of the relationship between the Green-Lagrange strain and the Cauchy-Green stretch ($\mathbf{E} = (\mathbf{C} - \mathbf{I})/2$). Also observing that all the 6 previous models can be expressed by Eq. (27), one introduces the fiber's strain energy (in a spread way), directly in the format of Eq. (27) allowing exponential improvements. This enables enhancing the isotropic Hartmann-Neff-Rivlin-Saunders isotropic strain energy, to reproduce general orthotropic materials as:

$$W = \hat{W} + \bar{W}^{isoc} + W^{fibers} = \underbrace{\frac{K}{8n^2}\left(J^{2n} + J^{-2n} - 2\right) + \frac{G}{4}\left\{\left(\bar{I}_1 - 3\right) + \left(\bar{I}_2 - 3\right)\right\}}_{Hartmann-Neff-Rivlin-Saunders\,isotropic} +$$
$$+ \underbrace{\left(\frac{R_1}{\alpha_1 + 1} E_{11}^{\alpha_1 + 1} + \frac{R_2}{\alpha_2 + 1} E_{22}^{\alpha_2 + 1} + \frac{R_3}{\alpha_3 + 1} E_{33}^{\alpha_3 + 1} \right)}_{Longitudinal\ fiber\ stiffness} + \tag{42}$$
$$+ \underbrace{2\left[\frac{\left(R_{1(12)} + R_{2(21)}\right)}{\gamma_{12} + 1} E_{12}^{\gamma_{12}+1} + \frac{\left(R_{1(13)} + R_{3(31)}\right)}{\gamma_{13} + 1} E_{13}^{\gamma_{13}+1} + \frac{\left(R_{2(23)} + R_{3(32)}\right)}{\gamma_{23} + 1} E_{23}^{\gamma_{23}+1} \right]}_{Shear\ fiber\ stiffness}$$

in which $\hat{W} + \bar{W}^{isoc}$ is called the Hartmann-Neff-Rivlin-Saunders isotropic constitutive model (Rivlin and Saunders, 1951; Hartmann and Neff, 2003; Kishino et al., 2022). When $\alpha_i = 1$ and $\gamma_{ij} = 1$, the energy of elastic fibers (W^{fibers}) is simply the one-dimensional SVK model including shear stiffness, that can also be written as Eq. (27) in its pure format. This procedure recovers the Tailoring technique described in section 6 with fibers following the orthotropic directions when $R_{i(i\ell)} = 0$ resulting into a unique shear modulus at small strains, corresponding to the isotropic matrix shear modulus.

The integer parameters α_i and γ_{ij} may also be used to calibrate the large strain behavior of the model, see example 5. The fiber's elastic constants are calculated as:

$$R_i = \mathcal{E}_i \left(a_{(i)}^{fibers} / a_{(i)}^{cont} \right)$$

and

$$R_{i(i\ell)} = G_{i(i\ell)} \left(a_{(i)}^{fibers} / a_{(i)}^{cont} \right) \tag{43}$$

in which $\mathcal{E}_i$ is the elastic modulus of fiber following direction $\vec{o}_i$, $G_{i(i\ell)}$ is the shear modulus of fibers that follow direction i and give shear stiffness for plane $i\ell$ and $a_{(i)}^{fibers} / a_{(i)}^{cont}$ is the area fraction between fibers and matrix for a given direction i. It is important to mention that, for example, $G_{1(12)}$ is not necessarily equal to $G_{2(21)}$ introducing a dependence of the fiber's cross section shapeson the shear behavior of material. The convexity of the proposed model is guaranteed by its isotropic part.

4.8 Model (h) Homogenized model with Almansi-like fibers

This model follows the same idea of model (g) (with $\alpha_i = 1$ and $\gamma_{ij} = 1$) and, in this case, the isolated fiber's energy is also convex in compression. In order to write this model one substitutes the longitudinal part of the fibers' SVK-like strain energy of model (g) by the one-dimensional Almansi-like strain energy, given by:

$$W_{AL}^{fibers} = \frac{R_1}{4}\left[\left(2E_{11}+1\right) - \ln\left(2E_{11}+1\right) - 1\right] + \frac{R_2}{4}\left[\left(2E_{22}+1\right) - \ln\left(2E_{22}+1\right) - 1\right]$$
$$+ \frac{R_3}{4}\left[\left(2E_{33}+1\right) - \ln\left(2E_{33}+1\right) - 1\right] + \tag{44}$$
$$+ \left[\left(R_{1(12)} + R_{2(21)}\right)E_{12}^2 + \left(R_{1(13)} + R_{3(31)}\right)E_{13}^2 + \left(R_{2(23)} + R_{3(32)}\right)E_{23}^2\right]$$

in which R_i and $R_{i(i\ell)}$ have the same meaning described by Eq. (43). This is the only case strain energy function cannot be writtenin the same format of Eq. (27), but opens the possibility to write new models taking advantage of exponential functions (Holzapfel and Ogden, 2009;Avazmohammadi et al., 2019).

Remarks

Models (b), (c), and (d) are equivalent; however, the use of model (d) simplifies the characterization of part of elastic constants by usual small strain's experimental tests. The analysis of model (a) indicates that the minimum parameter choice is not the best one. It introduces more steps to find elastic constants and limits the range of covered materials. However, it is an important mathematical exercise that should not be forgotten. Model (e) differs from model (d) only at the large strain range, but not using the separation of isochoric from volumetric strains complicates developing simple elastoplastic models for homogeneous orthotropic materials at large strains as proposed by Coda (2021) and Coda and Sanches (2022) for isotropic materials. Model (f) introduces a new parameter that opens the possibility of using models (d) and (e) at the same time. Models (g) and (h) illustrate how to reproduce large strain tailoring strategies by continuous orthotropic material modeling. These models are useful when one knows the fiber/matrix volume fraction and the mechanical properties of isolated employed materials, or when materials are notably constituted by fiber/matrix arrangements and the mechanical properties can be experimentally evaluated. In this study models (g), (h) or discrete tailoring are also used to show how to calculate ground properties for models (d), (e) and (f) from simple linear elastic experiments.

5 NUMERICAL IMPLEMENTATION - CONTINUUM

Although the study concern is not to solve large examples, the finite element method is used as a tool to validate the proposed constitutive models. The operational version of the FEM presented here has already been widely tested in several linear and nonlinear representative structural cases by Soares et al (2021), Coda (2021), Paccola and Coda (2020) and Paccola et al (2015), for instance.

Onestart the numerical modeling of nonlinear elastic mechanical problems from the weak equilibrium equation in its Lagrangian form as Ogden (1984) and Bonet and Wood (1997):

$$\delta\Pi = \int_{V_0} \rho_0 \ddot{\vec{y}} \cdot \delta\vec{y}\, dV_0 - \int_{V_0} \vec{b}^0 \cdot \delta\vec{y}\, dV_0 - \int_{\Gamma_0} \vec{p}_0 \cdot \delta\vec{y}\; dS_0 + \int_{V_0} \boldsymbol{S} : \delta\boldsymbol{E}\, dV_0 = 0 \tag{45}$$

in which Π is the total mechanical energy of the system $\vec{b}_0$ and $\vec{p}_0$ are two point functions, i.e., mapped in the initial coordinates $\vec{x}$ acting in current coordinates $\vec{y}$, $\boldsymbol{S}$ is the second Piola-Kirchhoff stress and $\ddot{\vec{y}}$ is the acceleration. The adopted Finite Element formulation uses nodal positions as degrees of freedom making simple to model geometric nonlinear mechanical problems and curved elements for linear and nonlinear applications, thus the deformation function $\vec{f}$ is written by the composition of two numerical mappings, see Fig. 2, as

$$\vec{f} = \vec{f} \circ \left(\vec{f}^0\right)^{-1} \tag{46}$$

with

$$f_i^0 = x_i = \phi_\alpha\left(\vec{\xi}\right) X_i^\alpha$$

and

$$f_i^1 = y_i = \phi_\alpha\left(\vec{\xi}\right) Y_i^\alpha \tag{47}$$

in which ϕ_α are usual FEM shape functions associated with node α, $\vec{\xi}$ are the set of dimensionless coordinates, X_i^α are nodal initial coordinates and Y_i^α are current nodal positions. The current nodal positions are actually the FEM degrees of freedom; therefore the adopted element has three degrees of freedom per node.

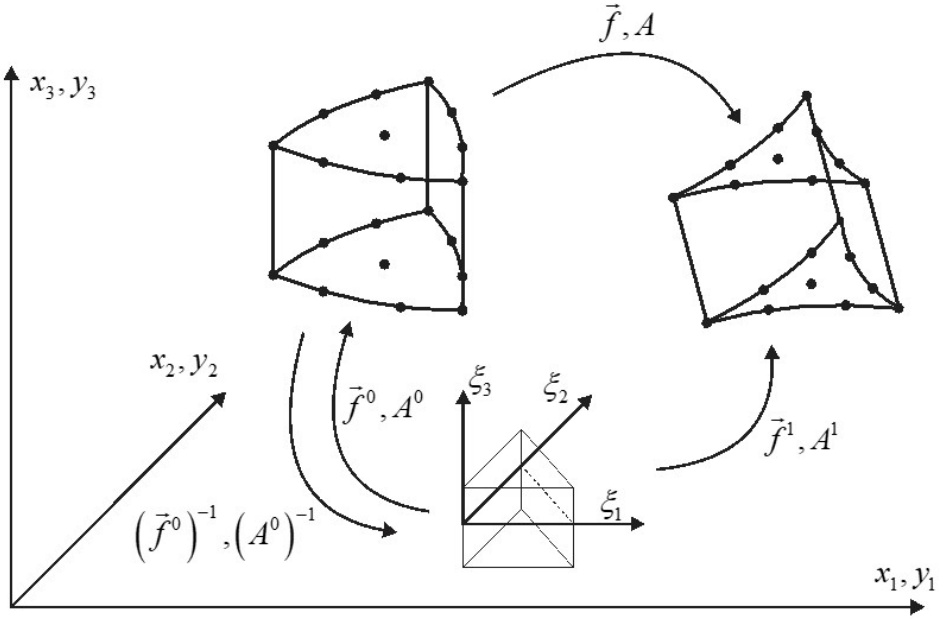

Figure 2 *Finite element deformation as a function of initial and current mappings.*

From Eq. (46) the deformation gradient is numerically given by:

$$\boldsymbol{A} = \boldsymbol{A}^1 \cdot \left(\boldsymbol{A}^0\right)^{-1} \tag{48}$$

with

$$A_{ij}^0 = \frac{\partial x_i}{\partial \xi_j}$$

and

$$A_{ij}^1 = \frac{\partial y_i}{\partial \xi_j} \tag{49}$$

Writing the Green-Lagrange strain variation $\delta \boldsymbol{E}$ as a function of the current nodal position variation $\delta \vec{Y}$, i.e.,

$$\delta \boldsymbol{E} = \frac{\partial \boldsymbol{E}}{\partial \vec{Y}} \cdot \delta \vec{Y} \,. \tag{50}$$

one is able to write the numerical weak form of equilibrium, Eq. (45), as:

$$\left(\int_{V_0} \rho_0 \, \phi \otimes \phi \, dV_0 \cdot \ddot{\vec{Y}} - \int_{V_0} \phi \otimes \phi \, dV_0 \cdot \vec{B}^0 - \int_{S_0} \varphi \otimes \varphi \; dS_0 \cdot \vec{P} + \int_{V_0} \boldsymbol{S}^c : \frac{\partial \boldsymbol{E}}{\partial \vec{Y}} \, dV_0 \right) \cdot \delta \vec{Y} = 0 \tag{51}$$

in which φ are surface shape functions.

As $\delta\vec{Y}$ is arbitrary, after numerical integration, Eq. (51) results,

$$M \cdot \ddot{\vec{Y}} + \vec{F}^{int}(\vec{Y}) - \vec{F}^{ext} = \vec{0} \tag{52}$$

in which $\vec{F}^{ext}$ represents applied forces, $\vec{F}^{\text{int}}(\vec{Y})$ are internal forces that depends on current nodal positions and involves the developed constitutive models and $M \cdot \ddot{\vec{Y}}$ corresponds to inertial forces that will be not considered in this study. More details regarding the solution of Eq. (52) can be seen, for instance, in Coda (2021), Coda and Sanches (2022) and Soares et al (2021).

6 TAILORING MODEL – IMMERSION OF FIBERS INTO CONTINUUM

This section describes the Tailoring technique employed to couple fiber elements inside the continuum element. It can be used to model random immersed fibers, but here only orthotropic materials are considered. To model the matrix of fiber-reinforced material, the Hartmann-Neff-Rivlin-Saunders model (Rivlin and Saunders, 1951; Hartmann and Neff, 2003; Kishino et al., 2022) - described in section 4.6 (Model (f)) - is adopted.

Immersed fibers don't increase the number of degrees of freedom, so without loss of generality, one models fibers' segments as truss elements. The change of configuration function ($\vec{f}$) of a truss (fiber) element is depicted in Fig. 3, in which L_0 and L the initial (reference) and the current element lengths, respectively. The one dimensional description of the fiber (truss) element indicates that scalar stress and strain are sufficient for its modeling. Thus, the Jacobian of the change of configuration function is L/L_0. In Fig. 3 one can see the initial and current positions of the truss element, which the change of configuration function is represented by $\vec{f}$. Nodes are also indicated to show the large rotation present in the kinematic description.

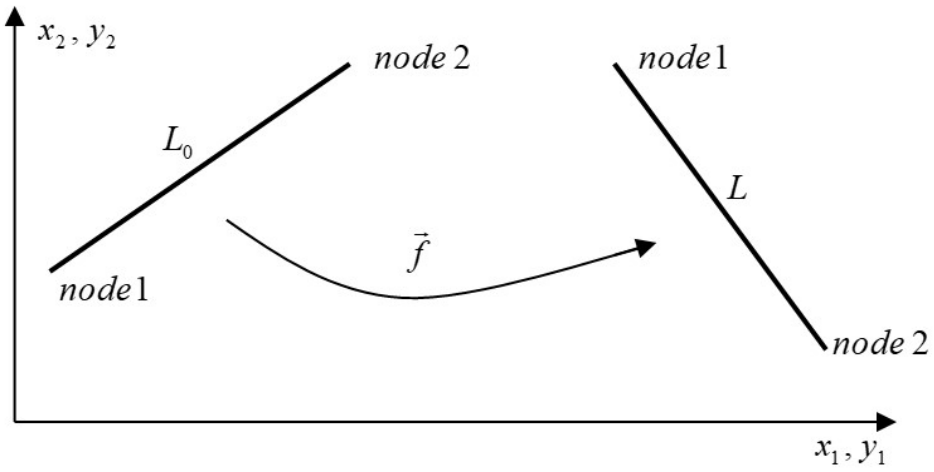

Figure 3 Change of configuration of a truss element

The relation between the Green-Lagrange strain and the nodal coordinates is given directly by:

$$E = \left(L^2 / L_0^2 - 1\right)/2 = \left[\left(\left(Y_1^2 - Y_1^1\right)^2 + \left(Y_2^2 - Y_2^1\right)^2 + \left(Y_3^2 - Y_3^1\right)^2\right)/L_0^2 - 1\right]/2 \tag{53}$$

Where Y_i^k is the current coordinate of node k in direction i, i.e., the degrees of freedom to be eliminated in the immersion process. The adopted strain energies are the one-dimensional SVK and the one-dimensional Alamansi-like models, given by:

$$w_{SVK}(Y_i^k) = \frac{1}{2}\mathbb{E}\left(E\left(Y_i^k\right)\right)^2$$

or

$$w_{AL} = \frac{\mathbb{E}}{4}\left[\left(2E+1\right) - \ln\left(2E+1\right) - 1\right] \tag{54}$$

in which $\mathbb{E}$ is the longitudinal elastic modulus. From these expressions, one writes the complete truss positional FEM formulation (Coda and Greco, 2004).

As the specific strain energy of a truss element ℓ is constant, the strain energy of one element is given by:

$$W_{SVK}(Y_i^k) = \mathbb{E}\left(A_0 L_0\right)^{\ell}\left(E(Y_i^k)\right)^2 / 2$$

or

$$W_{AL} = \mathbb{E}\left(A_0 L_0\right)^{\ell}\left[\left(2E+1\right) - \ln\left(2E+1\right) - 1\right] / 4 \tag{55}$$

where A_0 is the cross section area.

The immersion is understood observing Fig. 4, i.e., a solid finite element undergoes a change of configuration with a fiber (truss element) immersed in its interior.

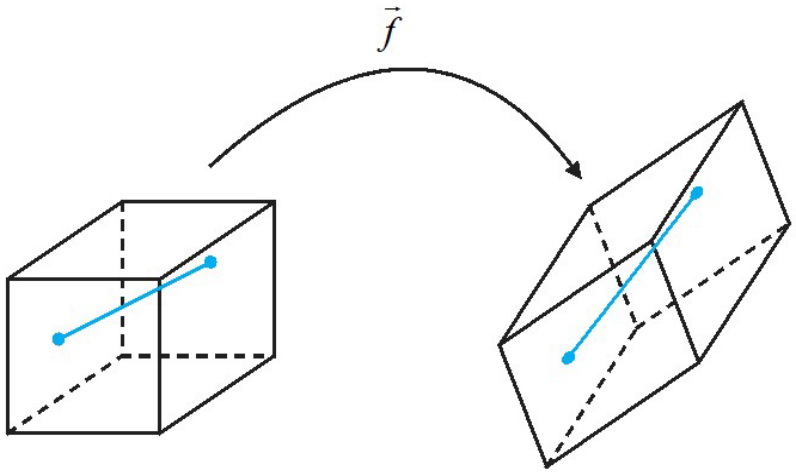

Figure 4 Change of configuration of a fiber conditioned to the solid element movement

As long as the movement of the fiber nodes is conditioned to the movement of the solid element nodes the strain energy of the fiber can be added to the strain energy of the solid as described below. The conditioning of the fiber element movement regarding the solid movement is performed by writing the truss nodes' degrees of freedom (current positions) as functions of the solid nodes' degrees of freedom (solid nodes current positions). Using Eq. (47), rewritten here for a particular dimensionless coordinate $\vec{\xi}^{\,p}$, results

$$\hat{X}_i^p = \phi^m(\vec{\xi}^{\,p})X_i^m$$

and

$$\hat{Y}_i^p = \phi^m(\vec{\xi}^p) Y_i^m \tag{56}$$

in which the upper hat $\hat{\bullet}$ indicates immersed coordinate and superscript p indicates fiber nodes that will disappear of the system of equations. The determination of $\vec{\xi}^p$ is automatically done from the known initial nodes position, inverting the first system of equations present in Eq. (56). Substituting Eq. (56) into Eq. (55) results:

$$W^\ell = W^\ell(\phi^m(\vec{\xi}^p) Y_i^m) \tag{57}$$

i.e., the strain energy of an immersed fiber element ℓ (it can be SVK or Almansi) is written as a function of current nodal coordinates of a solid element. When various fiber elements are immersed results:

$$W^{fiber} = \sum_{\ell}^{n\ell} W^\ell(\phi^m(\vec{\xi}^p) Y_i^m) \tag{58}$$

in which $n\ell$ is the number of immersed fiber elements and Y_i^m are the solid element degrees of freedom. The solid internal force is given by the derivative of the strain energy regarding solid degrees of freedom, thus, by the chain rule one write as Paccola et al. (2015), Sampaio et al. (2015) and Paccola and Coda (2020):

$$f_\gamma^{\text{int}\,\alpha} = \frac{\partial W^{fiber}}{\partial Y_\gamma^\alpha} = \frac{\partial}{\partial Y_\gamma^\alpha} \sum_{\ell=1}^{n\ell} W^\ell(\hat{Y}_i^p) = \sum_{\ell=1}^{n\ell} \frac{\partial W^\ell}{\partial \hat{Y}_i^p} \frac{\partial(\phi^m(\vec{\xi}^p) Y_i^m)}{\partial Y_\gamma^\alpha} = \sum_{\ell=1}^{n\ell} \frac{\partial W^\ell}{\partial \hat{Y}_i^p} \phi^\alpha(\vec{\xi}^p) \delta_{\gamma i} \tag{59}$$

or

$$f_\gamma^{\text{int}\,\alpha} = \sum_{\ell=1}^{n\ell} \left(\hat{f}_i^{\text{int}\,p} \Psi_{i\gamma}^{p\alpha} \right)^\ell \tag{60}$$

i.e., the internal fiber force $f_\gamma^{\text{int}\,\alpha}$ energy conjugate to the solid element is given by a sum of ordinary fiber elements internal forces $\hat{f}_\gamma^{\text{int}\,p}$ weighted by the transformation tensor $\boldsymbol{\Psi}_{i\gamma}^{p\alpha} = \phi^\alpha(\vec{\xi}^p)\delta_{\gamma i}$ that corresponds to the shape function of node α calculated at the immerse node dimensionless position $\vec{\xi}^p$.

Performing the second derivative of the strain energy results the fiber Hessian matrix conjugate to solid degrees of freedom:

$$H_{\gamma\eta}^{\alpha\beta} = \sum_{\ell=1}^{n\ell} \left(\hat{H}_{ij}^{pq} \left[\phi^\alpha(\vec{\xi}^p)\delta_{\gamma i} \right] \left[\phi^\beta(\vec{\xi}^q)\delta_{\eta j} \right] \right)^\ell$$

or

$$H_{\gamma\eta}^{\alpha\beta} = \sum_{\ell=1}^{n\ell} \left(\Psi_{i\gamma}^{p\alpha} \hat{H}_{ij}^{pq} \Psi_{j\eta}^{q\beta} \right)^\ell \tag{61}$$

in which $\hat{H}_{ij}^{pq}$ is the ordinary Hessian matrix of the immersed fiber ℓ and the weighting has the same meaning described for internal forces.

7 EXAMPLES

In this section the tailoring strategy is used as a starting point to validate the homogenized models (g) and (h). After that, these models are used to make fictitious experiments at small strains, from which ground constants for models (d), (e) and (f) and show their behavior at large strains are computed. Finallythe simulation of a pig myocardium tissue in order to show the possibilities of model (g) is carried out. For all examples a cube with unitary dimensions and simple linear element discretizations is used. Although our finite element implementation is capable of solving problems with complex geometries, this is not the objective of this study.

7.1 Example 1 – Validating models (g) and (h) using tailoring models as reference

The geometry of this example is a cube with $1mm$ of side and a distribution of $50X50$ fibers (in each orthotropic direction) with $4x10^{-5}mm^2$ of area each. These fibers' areas are directed used in the tailoring model (Fig. 5b) as real fibers. From these fibers' areas and spread quantities one calculates the relation $a_{(i)}^{fibers} / a_{(i)}^{cont}$ for each fiber direction i, resulting in equal values of 0.1 for all orthotropic directions. The isotropic (Hartmann-Neff-Rivlin-Saunders) matrix properties –used for models (g), (h) and tailoring – are $E_{matrix} = 5N/mm^2$ and $\nu_{matrix} = 0.25$; resulting (from usual relations) in $K_{matrix} = 3.333N/mm^2$ and $G_{matrix} = 2N/mm^2$. The fibers' properties are $E_{fiber1} = 30N/mm^2$, $E_{fiber2} = 50N/mm^2$ and $E_{fiber3} = 10N/mm^2$. From these values and Eq. (43) one finds $R_1 = 3N/mm^2$, $R_2 = 5N/mm^2$, $R_3 = 1N/mm^2$ and $R_{i(i\ell)} = 0$ The last value is null because the tailoring model doesn't includes shear stiffness for fibers and the objective of this example is to compare models (g) and (h) with the tailoring model. When using model (g) - in this example - $\alpha_i = 1$ and $\gamma_{ij} = 1$ are adopted, i.e., the usual SVK model for fibers.

Formodels (g) and (h), discretizations are very simple (linear prismatic elements), see Fig. 5(a), as the intention is to exclude any geometrical influence from the material behavior.

The performed stretching follows direction $\vec{i}$ and the fibers' directions alternate within directions $\vec{i}$, $\vec{j}$ and $\vec{k}$ in order to verify the representative continuous models, i.e., if orthotropic direction 1 coincides with direction $\vec{i}$ oneapplies λ_1 measuring S_{11}^{fiber}, S_{22}^{fiber} and S_{33}^{fiber} and so on. Shear tests are preformed constraining all nodes and applying relative translations between planes (no alternation of fiber's directions is performed). For example, the Green-Lagrange strain E_{12} is achieved by making a relative movement of planes orthogonal to direction 1 following direction 2 and strain E_{21} is achieved by a relative movement of planes orthogonal to direction 2 following direction 1.

Fig. 5(b) presents the adopted discretization for the tailoring strategy (in which tetrahedral elements are employed from the adopted computational code) that is also simple, but more elaborated as it is important to keep symmetry in order to guaranty the representative volume. Tests for the tailoring strategy are also performed by fiber direction permutation.

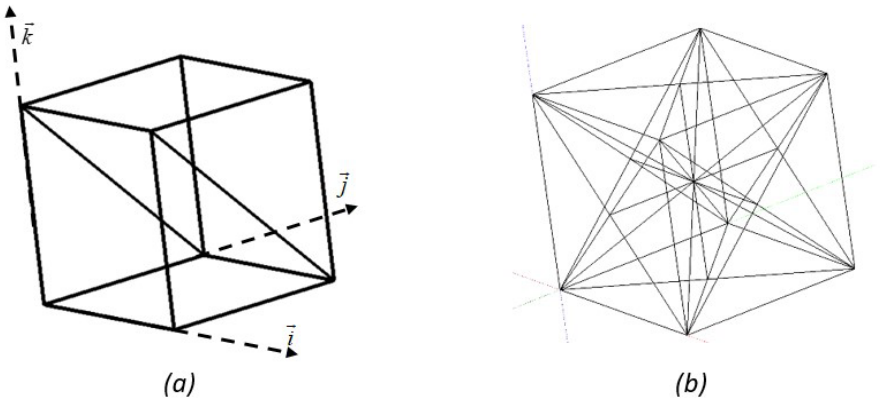

Figure 5 (a) ModelsSVK (g) andAlmansi (h) discretization, (b) Tailoring model discretization - planes ik, jk and ij are sliding for stretch tests following direction $\vec{i}$.

Fig. 6 shows, for models SVK (g) and Almansi (h) the second Piola-Kirchhoff stress at fibers for an applied stretching following orthotropic directions. As expectedfibers in the stretching direction present positive stresses while the other fibers suffer compression due to the matrix Poisson'sshortening at other directions.The corresponding tailoring models (SVK and Almansi) results are not shown because they are practically equal to the results of the continuous models SVK (g) and Almansi (h). From this observation models (g) and (h) are validated for stretching, i.e., the strategy used to introduce fibers in a continuum way is verified.

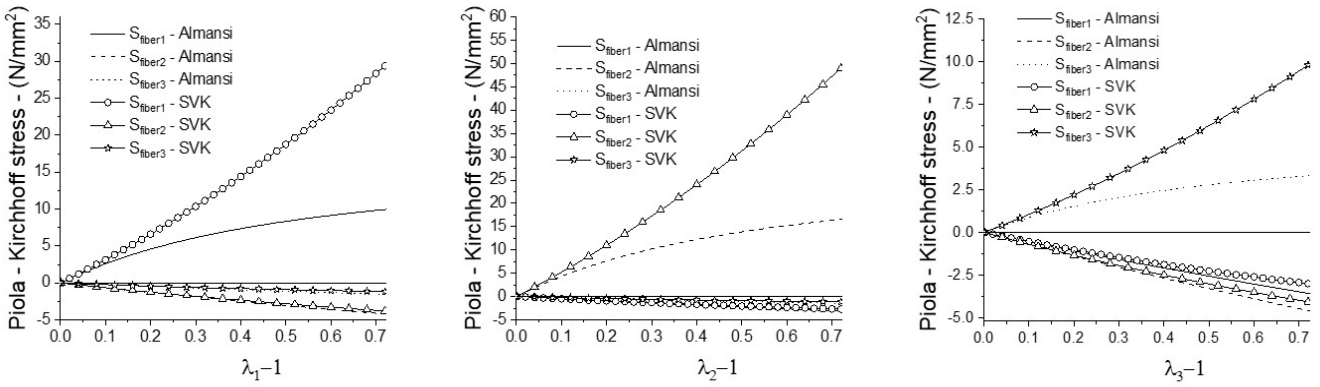

(a) Stretch following direction 1 *(b) Stretch following direction 2* *(c) Stretch following direction 3*

Figure 6 Piola-Kirchhoff stress at fibers for stretching (tension) following orthotropic directions

Fig. 7shows results for models SVK (g), Almansi (h) and tailoring when compression takes place in the main fiber directions. In this case results are also coincident until the tailoring strategy looses stability. To identify the instability points,Fig. 7 uses a black star over the complete curve of the continuous Almansi model (h) and a black square over the complete curve of the continuous SVKmodel (g). The instability occurs at the central point of the tetrahedral discretization forming a shear band. As the tailoring model is used as benchmark (Paccola et al (2015) and Coda and Paccola (2020)) and results are practically coincident for compression, one understands that the proposed continuum strategy is also validated in compression.

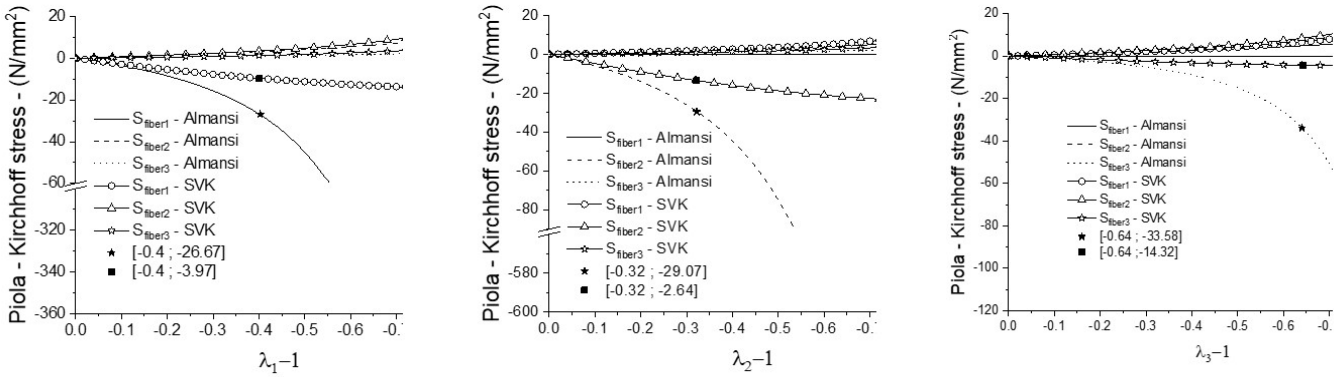

(a) Compression following direction 1 *(b) Compression following direction 2* *(c) Compression following direction 3*

Figure 7 Piola-Kirchhoff stress at fibers for compression following orthotropic directions

Fig. 8shows the shear stress results for imposed shear strains. From Fig. 7 and Fig. 6 one expects (and it is confirmed) that results of the tailoring model also coincides with continuous models SVK (g) and Almansi (h) in shear situations. In this case, as fibers are always stretched, no loss of stability occurs for the tailoring strategy. As tailoring results coincide with the proposed models in all applications one concludes that the proposed continuum models are validated.

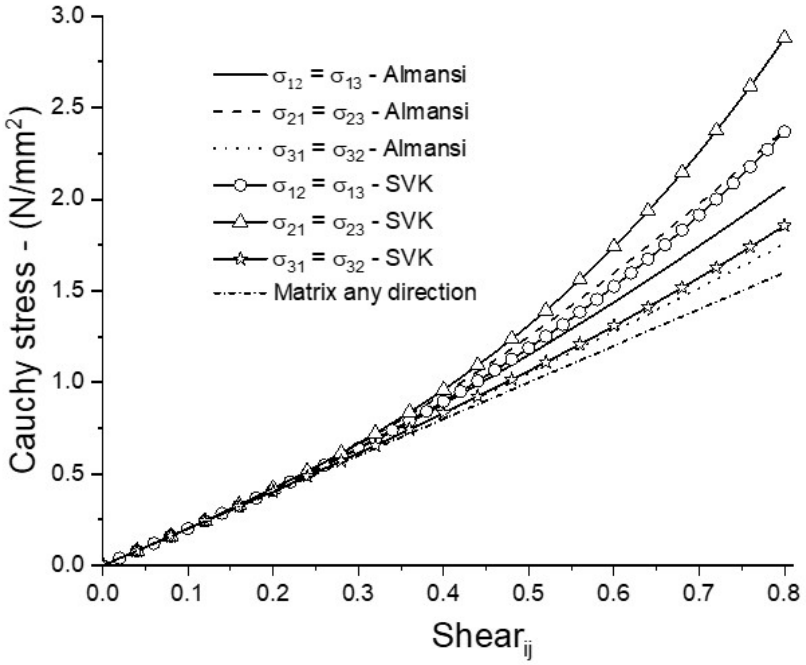

Figure 8 Shear stress versus shear strain γ_{ij} for SVK (g) and Almansi (h) models

It is also interesting to note thatin Fig. 8 the shear stiffness is growing as the shear strain grows. It occurs because fibers are stretching during shear. From this observation it was possible to propose $\alpha_i \neq 1$ and $\gamma_i \neq 1$ in model SVK (g), opening the possibility to reproduce the experimental result presented in example 5. Other interesting features presented in Fig. 8 are the equalities $\sigma_{12} = \sigma_{13}$, $\sigma_{21} = \sigma_{23}$ and $\sigma_{31} = \sigma_{32}$. They occur because for small strains shear stiffness depends only on the isotropic matrix and for large strains it depends on which fiber is being stretched. Fig. 14 of example 5 gives a geometrical clue to understand this observation.

7.2 Example 2 – Material Characterization for models (d), (e) and (f) from the material employed in example 1

Example 1 defines an orthotropic material via tailoring discretization in which “real” fibers are spread inside the domain. Example 1 also tests continuous models (SVK (g) and Almansi (h)) that use specific enhancements to substitute discrete fibers. In this example the material generated in the previous example is usedto extract- at small strainrange - elastic constants for models (d), (e) and (f). The proposition of these models intends to interconnect large strains and small strains orthotropic relations, something missing in the consulted literature. In order to do so one writes the compliance matrix (see Eq. A1) in a simplified way (small strains), as follows:

$$\begin{Bmatrix} \varepsilon_{11} \\ \varepsilon_{22} \\ \varepsilon_{33} \\ \varepsilon_{12} \\ \varepsilon_{13} \\ \varepsilon_{23} \end{Bmatrix} = \begin{bmatrix} d_{11} & d_{12} & d_{13} & 0 & 0 & 0 \\ d_{12} & d_{22} & d_{23} & 0 & 0 & 0 \\ d_{13} & d_{23} & d_{33} & 0 & 0 & 0 \\ 0 & 0 & 0 & 1/2G & 0 & 0 \\ 0 & 0 & 0 & 0 & 1/2G & 0 \\ 0 & 0 & 0 & 0 & 0 & 1/2G \end{bmatrix} \begin{Bmatrix} \sigma_{11} \\ \sigma_{22} \\ \sigma_{33} \\ \sigma_{23} \\ \sigma_{13} \\ \sigma_{12} \end{Bmatrix} \tag{62}$$

Fibers of the tailoring model do not work regarding shear at small distortions, thus the shear modulus at small strains is the same in all directions and equal to the matrix material shear modulus.

Applying $\sigma_{11} = 1.65x10^{-3} MPa$, $\sigma_{22} = 0$ and $\sigma_{33} = 0$ on the unitary cube of example 1, one achieves ε_{11}, ε_{22} and ε_{33}. Using Eq. (62) one finds the compliance values:

$$\varepsilon_{11} = 2.0x10^{-4} = \sigma_{11} d_{11} = \left(1.65x10^{-3}\ MPa\right) d_{11} \qquad \Rightarrow \qquad d_{11} = 1.21x10^{-1} / MPa$$

$$\varepsilon_{22} = -2.7x10^{-5} = \sigma_{11} d_{12} = \left(1.65x10^{-3} MPa\right) d_{12} \qquad \Rightarrow \qquad d_{12} = -1.66x10^{-2} / MPa$$

$$\varepsilon_{33} = -4.9x10^{-5} = \sigma_{11} d_{13} = \left(1.65x10^{-3} MPa\right) d_{13} \qquad \Rightarrow \qquad d_{13} = -2.99x10^{-2} / MPa$$

Following the same procedure and applying $\sigma_{11} = 0$, $\sigma_{22} = 2.04x10^{-3} MPa$ one achieves:

$$\varepsilon_{22} = 2.0x10^{-4} = \sigma_{22} d_{22} = \left(2.04x10^{-3} MPa\right) d_{22} \qquad \Rightarrow \qquad d_{22} = 9.82x10^{-2} / MPa$$

$$\varepsilon_{33} = -4.7x10^{-5} = \sigma_{22} d_{23} = \left(2.04x10^{-3} MPa\right) d_{23} \qquad \Rightarrow \qquad d_{23} = -2.33x10^{-2} / MPa$$

Finally, applying $\sigma_{11} = 0$, $\sigma_{22} = 0$ and $\sigma_{33} = 1.27x10^{-3} MPa$ one achieves:

$$\varepsilon_{33} = 2.0x10^{-4} = \sigma_{33} d_{33} = \left(1.27x10^{-3} GPa\right) d_{33} \qquad \Rightarrow \qquad d_{33} = 1.58x10^{-1} / GPa$$

Inverting the compliance matrix, results the linear elastic constitutive tensor as:

$$\mathfrak{H}^0 = \begin{bmatrix} \mathfrak{H}^0_{1111} & \mathfrak{H}^0_{1122} & \mathfrak{H}^0_{1133} & 0 & 0 & 0 \\ & \mathfrak{H}^0_{2222} & \mathfrak{H}^0_{2233} & 0 & 0 & 0 \\ & & \mathfrak{H}^0_{3333} & 0 & 0 & 0 \\ & & & 2\mathfrak{H}^0_{2323} & 0 & 0 \\ & Sym & & & 2\mathfrak{H}^0_{1313} & 0 \\ & & & & & 2\mathfrak{H}^0_{1212} \end{bmatrix} = \begin{bmatrix} 9 & 2 & 2 & 0 & 0 & 0 \\ & 11 & 2 & 0 & 0 & 0 \\ & & 7 & 0 & 0 & 0 \\ & & & 4 & 0 & 0 \\ & Sym & & & 4 & 0 \\ & & & & & 4 \end{bmatrix} MPa \tag{63}$$

Using Eq. (16) one finds the bulk modulus $K = 4.333\text{MPa}$ and applying Eq. (34) results:

$$\overline{\mathfrak{H}}^0 = \begin{bmatrix} \overline{\mathfrak{H}}^0_{1111} & \overline{\mathfrak{H}}^0_{1122} & \overline{\mathfrak{H}}^0_{1133} & 0 & 0 & 0 \\ & \overline{\mathfrak{H}}^0_{2222} & \overline{\mathfrak{H}}^0_{2233} & 0 & 0 & 0 \\ & & \overline{\mathfrak{H}}^0_{3333} & 0 & 0 & 0 \\ & & & 2\overline{\mathfrak{H}}^0_{2323} & 0 & 0 \\ & Sym & & & 2\overline{\mathfrak{H}}^0_{1313} & 0 \\ & & & & & 2\overline{\mathfrak{H}}^0_{1212} \end{bmatrix} = \begin{bmatrix} 4.666 & -2.333 & -2.333 & 0 & 0 & 0 \\ & 6.666 & -2.333 & 0 & 0 & 0 \\ & & 2.666 & 0 & 0 & 0 \\ & & & 4 & 0 & 0 \\ & Sym & & & 4 & 0 \\ & & & & & 4 \end{bmatrix} MPa \tag{64}$$

These values are directly applied into Eqs. (36), (39) and (41) to run models (d), (e) and (f), respectively, in the next example. It is interesting to recall that model (d) uses volume invariant to control the growth condition and the SVK-like part is conditioned to isochoric Green-Lagrange strains. Model (e) uses the volume invariant to control the growth condition and uses regular Green-Lagrange strains at the remaining part of the strain energy. Model (f) is a mix of models (d) and (e).

7.3 Example 3 – Comparing the large strain behavior of models (d), (e) and (f) using ground constants characterized at example 2

The same dimensions and discretization (Fig. 5(a)) of examples 1 and 2 are employed in this example. Models (d), (e) and (f) are not expected to be similar to models SVK (g),Almansi (h) and tailoring for stretching at large strains, but models (d) and (e) are expected to have the same behavior (among each other) for isochoric shear.

In this example, using the elastic constants G and K, as well as the stiffness tensor $\overline{\mathcal{H}}^0$ extracted in example 2 from the material of example 1, the large strain behavior of models (d), (e) and (f) are compared.

The stretch behavior in the third orthotropic direction (x_3) and the evolution of transverse strains in directions x_1 and x_2 are depicted in Fig. 9. Figure 10 shows the shear behavior for models (d), (e) and (f). Figure 11 shows the models behavior in compression.

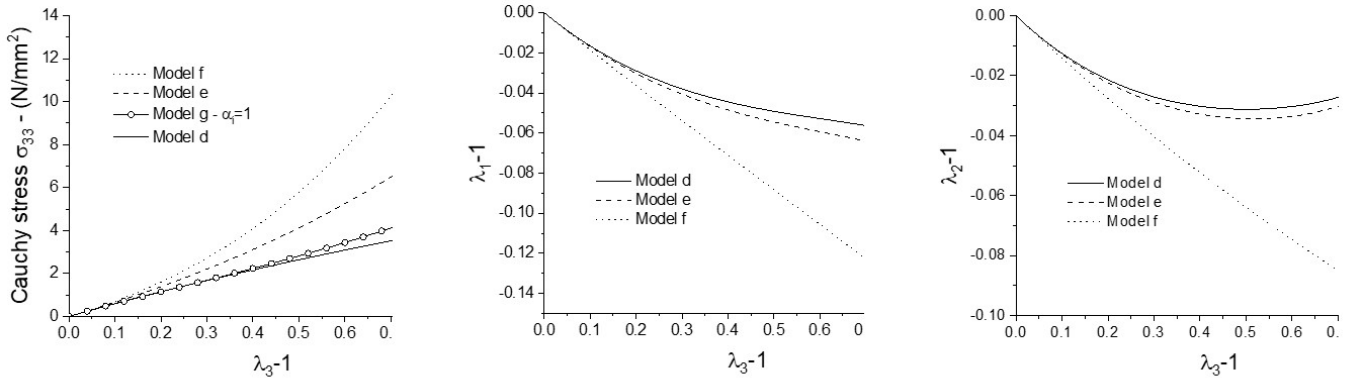

(a) Normal stress level (b) "Poisson's" behavior direction 1 (c) "Poisson's" behavior direction 2

Figure 9 Cauchy stress and Poisson's behavior for stretching applied in orthotropic direction 3

In Fig. 9(a) the stress behavior of model (g) is also introduced only as a scale reference. Comparing Figs. 9(b) and 9(c) one observes that the large stiffness in direction 2 has a larger influence in the "Poisson's" behavior. As expected, when the volume control diminishes (proportion of the volumetric strain energy) in the sequence of models (d), (e) and (f) the cross section of the specimen diminishes in a faster rate and the normal Cauchy stress grows accordingly in stretching.

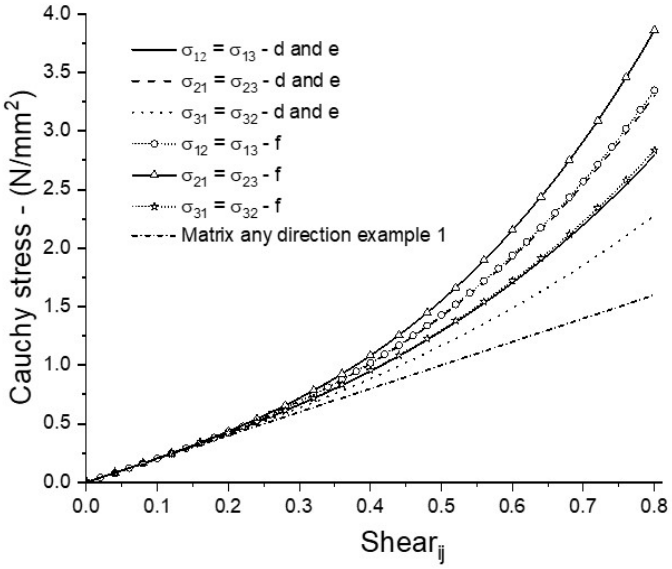

Figure 10 Shear stress behavior for models (d), (e) and (f)

As one can see in Fig. 10, regarding shear, model (f) has a stiffer behavior than models (d) and (e) meaning that parameter β (adopted as ½) can be used as a calibrating tool. Moreover, one confirms the expected equalities between models (d) and (e) in isochoric situations.

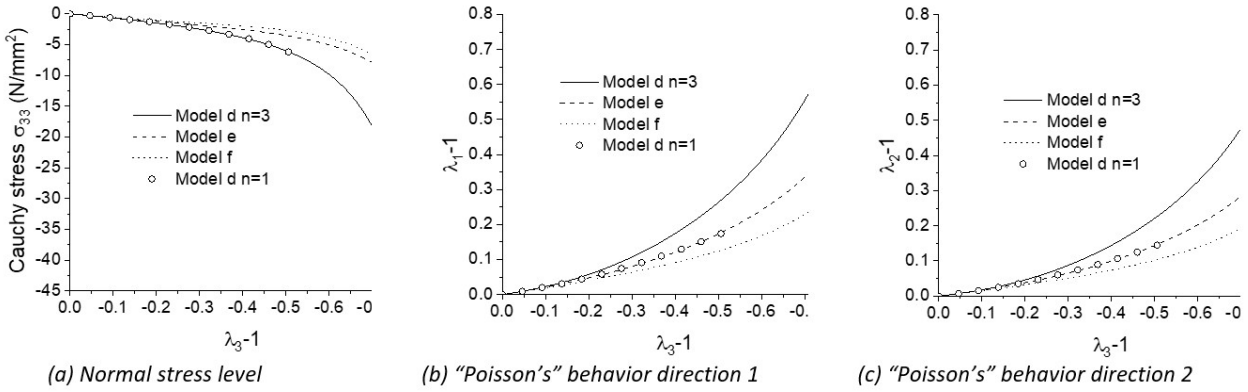

(a) Normal stress level *(b) "Poisson's" behavior direction 1* *(c) "Poisson's" behavior direction 2*

Figure 11 Cauchy stress and Poisson's behavior for compression applied in orthotropic direction 3

In Fig. 11the compression behavior of models are studied. It is possible to observe (Figs. 11(b) and 11(c)) that when using $n=1$ (see equation (12)) in model (d) the "Poisson's" behavior is similar to model (e), but with a higher stress level (Fig. 11(a)). This behavior leads to material instability (Ogden (1984)), provoking a shear banding in the numerical analysis of model (d). Adopting $n=3$ in model (d), the "Poisson's" behavior considerably increases, see Figs. 11(b) and 11(c). It provides a larger deformed "cross section" for the specimen, eliminating the shear banding for the same Cauchy stress level (Fig. 11(a)). In this example the contribution of parameter n becomes clear, i.e., when its value increases the deformed volumetric stiffness also increases.

7.4 Example 4 –Models (d), (e) and (f) with not equal shear modulus at small strain

As mentioned before the tailoring model is not able to represent (at small strains) different shear modulus. In order to show that the proposed models are more general than the tailoring one, in this example model (g) is used with the same fiber longitudinal elastic modulus and relation $a_{(i)}^{fibers}/a_{(i)}^{cont}=0.1$ for all orthotropic directions of example 1, but different fiber's shear modulus to extract (at small strains) different ground shear constants. The matrix properties are $E_{matrix}=5N/mm^2$ and $\nu_{matrix}=0.25$; resulting in $K_{matrix}=3.333N/mm^2$ and $G_{matrix}=2N/mm^2$. The fiber's properties are $E_{fiber1}=30N/mm^2$, $E_{fiber2}=50N/mm^2$, $E_{fiber3}=10N/mm^2$, $G_{fiber1}=20N/mm^2$, $G_{fiber2}=30N/mm^2$ and $G_{fiber3}=5N/mm^2$. From these values and Eq. (42) one finds $R_1=3N/mm^2$, $R_2=5N/mm^2$, $R_3=1N/mm^2$, $R_{1(12)}=2N/mm^2$, $R_{1(13)}=2N/mm^2$, $R_{2(21)}=3N/mm^2$, $R_{2(23)}=3N/mm^2$, $R_{3(31)}=0.5N/mm^2$ and $R_{3(32)}=0.5N/mm^2$.

Repeating the procedure of example 2 one finds the bulk modulus $K=4.333N/mm^2$ and

$$\bar{\mathcal{H}}^0=\begin{bmatrix} \bar{\mathcal{H}}^0_{1111} & \bar{\mathcal{H}}^0_{1122} & \bar{\mathcal{H}}^0_{1133} & 0 & 0 & 0 \\ & \bar{\mathcal{H}}^0_{2222} & \bar{\mathcal{H}}^0_{2233} & 0 & 0 & 0 \\ & & \bar{\mathcal{H}}^0_{3333} & 0 & 0 & 0 \\ & & & 2\bar{\mathcal{H}}^0_{2323} & 0 & 0 \\ & Sym & & & 2\bar{\mathcal{H}}^0_{1313} & 0 \\ & & & & & 2\bar{\mathcal{H}}^0_{1212} \end{bmatrix}=\begin{bmatrix} 4.666 & -2.333 & -2.333 & 0 & 0 & 0 \\ & 6.666 & -2.333 & 0 & 0 & 0 \\ & & 2.666 & 0 & 0 & 0 \\ & & & 14 & 0 & 0 \\ & Sym & & & 9 & 0 \\ & & & & & 11 \end{bmatrix} N/mm^2$$

These constants are used in models (d), (e) and (f) and the isochoric shear stress results are compared in Fig. 12. One should observe that in this case the obvious equality $\sigma_{ij}=\sigma_{ji}$ are easily identified at small strains, but for large strains the not so obvious equalities $\sigma_{31}=\sigma_{32}$, $\sigma_{21}=\sigma_{23}$ and $\sigma_{13}=\sigma_{12}$ (explained in example 5 for identical fiber shear modulus – Figs. 14 and 15) do not take place. It occurs due to different combinations among fiber stretching and shear stiffness.

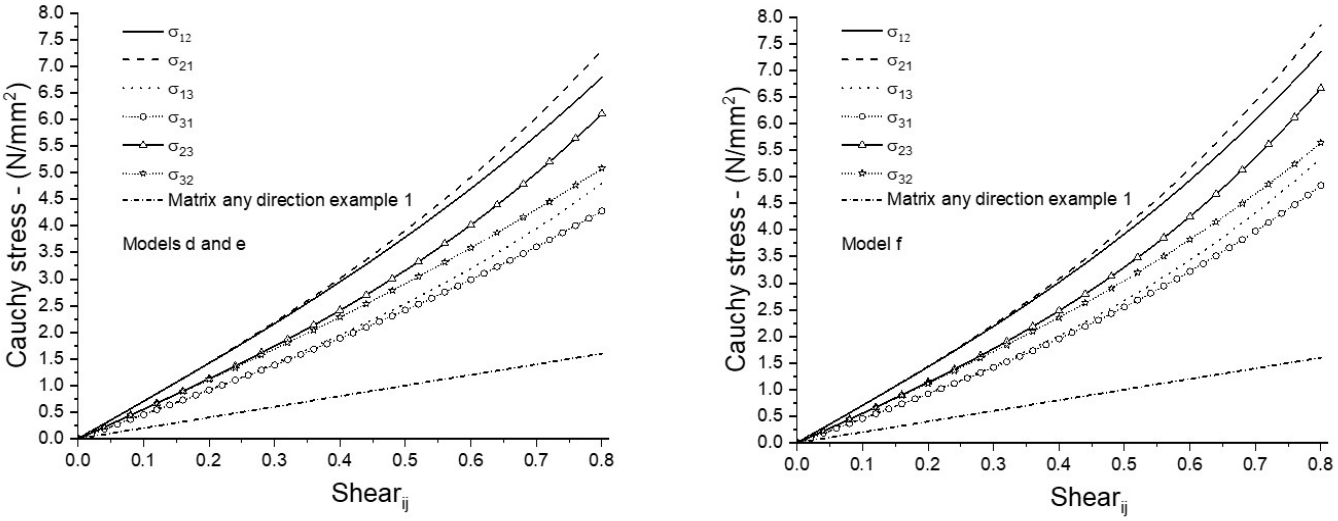

(a) Shear stress at large strain - models (d) and (e) *(b) Shear stress at large strain - model (f)*

Figure 12 Shear stress behavior for orthotropic material with different shear constants.

As previously mentioned, models (d) and (e) have the same behavior for isochoric strains, thus only one figure (Fig 12(a)) is presented for both models. These results allow calibrating and/or adapting models (d), (e), (f) or (g) to represent complex models. In particular, the existence of parameters α_i and γ_i gives more flexibility to model (g) and no adaptations are necessary. Thus model (g) is used in the next example to simulate the passive pig myocardium tissue experimentally tested by Dokos et al. (2002).

7.5 Example 5 – Modeling the passive pig myocardium using model (g)

This example uses experimental data provided by Dokos et al. (2002) and adapted by Holzapfel and Ogden (2009). It is used to show the possibility of adopting the proposed modelsto simulate general materials. The detailed description of the example indicates how an organized strategy facilitates to characterize the material. The behavior of model (g) in example 1 indicates that the increasing of shear modulus when pure distortion increases is direct related to fibers stretching and inclining. Observing in Dokos et al. (2002) that the pig myocardium tissue has an orthotropic characteristic with a preferential fiber direction and other two less important (secondary and tertiary), one identifies that model (g) presents the proper orthotropic stiffening to characterize the material.

The fiber set orientation can be seen in Fig. 13(a) in which directions s, n and f correspond to the orthotropic directions x_1, x_2 and x_3.

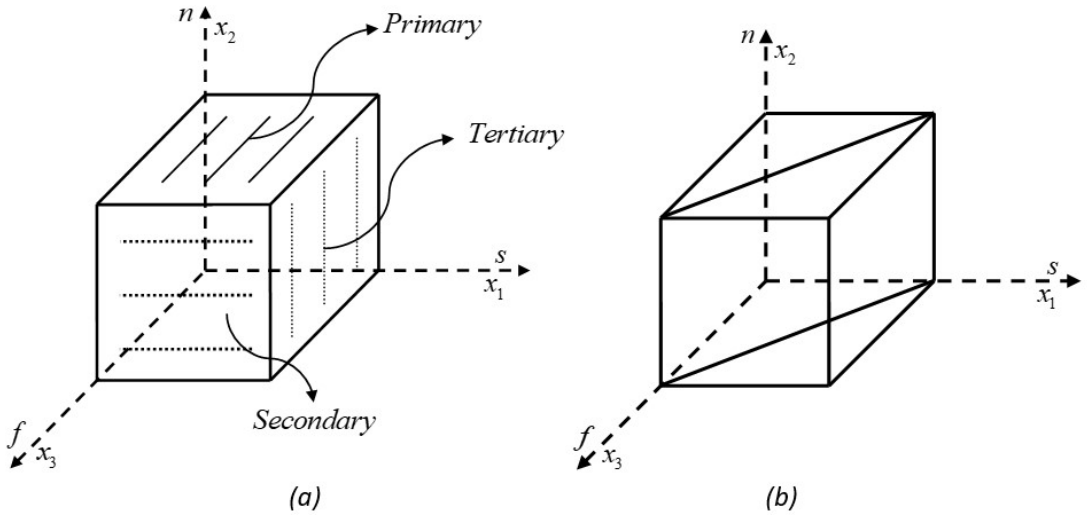

Figure 13 (a) Orientation of myocardium fibers and (b) Linear (8 nodes) discretization

In order to built stress-strain (pure distortion) curves, all possible shear strain displacements are imposed on a unitarycube. Strains are imposed controlling all nodes positions (eight) of the simple discretization presented in Fig. 13(b). The applied strain cases are schematically described in Fig. 14, all four nodes of the plane opposite to the fixed one are subject to the same displacement in the sense of the depicted arrows. Shear ij means that the plane orthogonal to direction i is moved in direction j. The corresponding letters s, n and f are also used following the notation adopted by Dokos et al. (2002) and Holzapfel and Ogden (2009).

As the homogeneous (matrix) part of model (g) has linear behavior for shear effects, it is easy to verify that the increasing of shear stiffness is given by the stretching of fibers. When there isn't different shear stiffness for fibers, one observes from Figs. 13(a) and 14 that: (i) the large strain behaviors of Shear 31 and Shear 32 are related to the stretching of the primary fiber set, (ii) the large strain behaviors of Shear 13 and Shear 12 are related to the stretching of the secondary fiber set, and (iii) the large strain behaviors of Shear 21 and Shear 23 are related to the to the stretching of the tertiary fiber set.

Differences among these behaviors given by the experimental result of Dokos et al. (2002) can be attributed to different fibers' shear stiffness (shape effect), not captured by the model proposed by Holzapfel and Ogden (2009) based only on strain invariants. The shape effect is inspired in the shear stiffness difference of bars when cross sections do not have regular shapes.

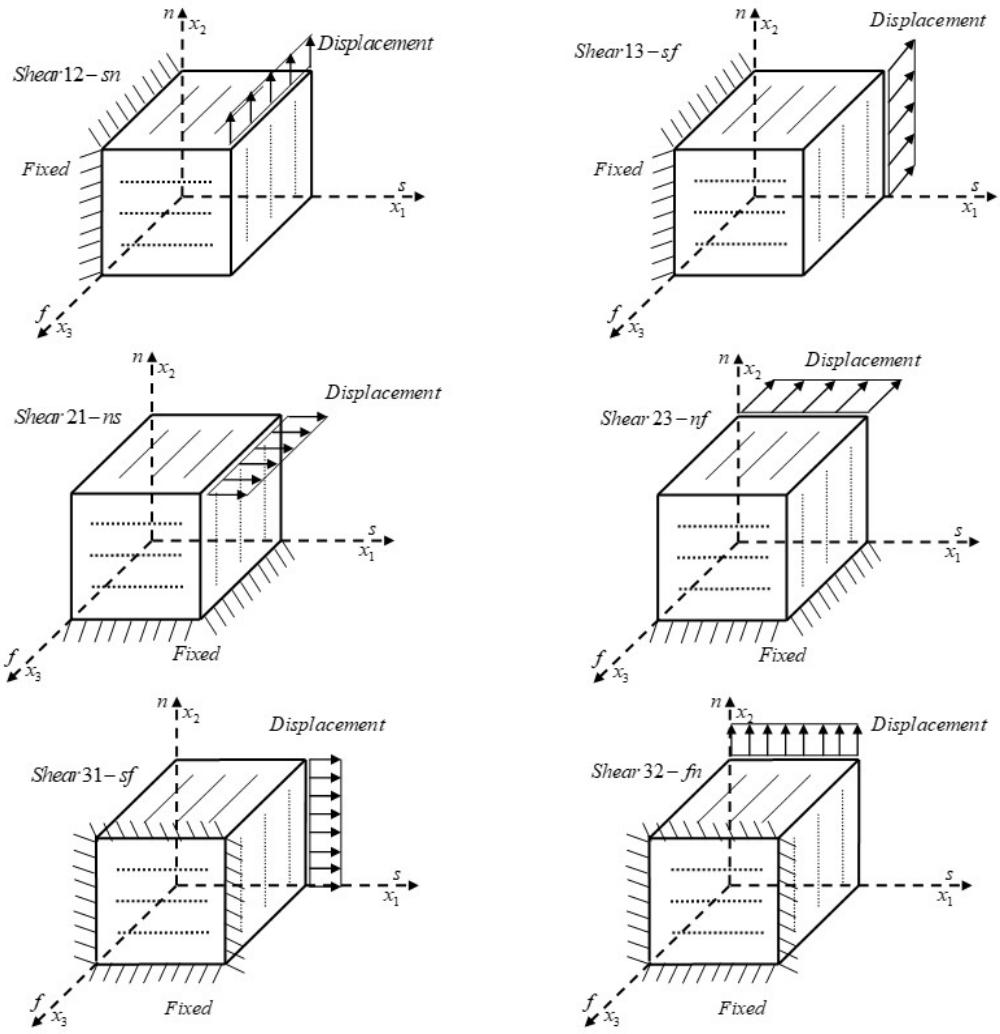

Figure 14 Schematically imposition of shear for linear discretization

In Fig. 15 results are compared with Holzapfel and Ogden (2009). The following constants for model (g) are adopted: $K = 4.67kPa$, $G = 0.5kPa$, $n = 1$, $\alpha_i = 2$, $\gamma_{ij} = 4$, $R_1 = 400kPa$, $R_2 = 100kPa$, $R_3 = 1860kPa$ and $R_{i(i\ell)} = 50kPa$. The last adopted constant corresponds to consider the same shear modulus (small strain) in all

directions, as the reference model is not able to do different. As mentioned before, this choice makes $\sigma_{13} = \sigma_{31}$, $\sigma_{12} = \sigma_{21}$ and $\sigma_{23} = \sigma_{32}$.

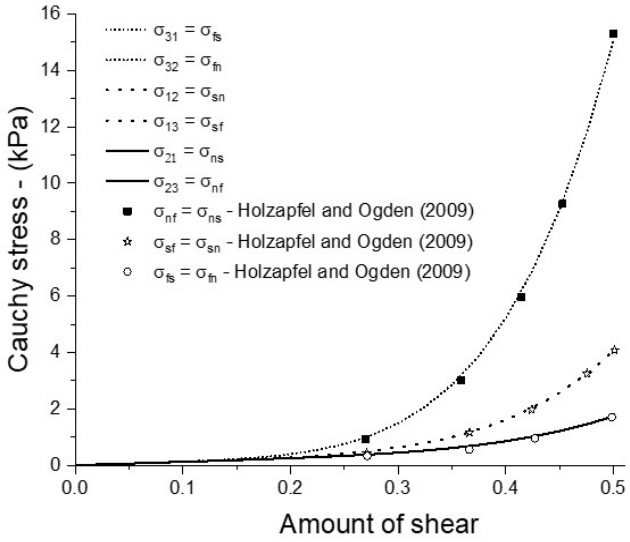

Figure 15 Comparing results of model (g) and numerical result presented by Holzapfel and Ogden (2009)

Results of Fig. 15 are in good agreement with the reference numerical solution and the expected results $\sigma_{13} \neq \sigma_{31}$, $\sigma_{12} \neq \sigma_{21}$ and $\sigma_{23} \neq \sigma_{32}$ for large strain range takes place. However, experimental results do not confirm equalities $\sigma_{fs} = \sigma_{fn}$, $\sigma_{sf} = \sigma_{sn}$ and $\sigma_{ns} = \sigma_{nf}$.

To show that the proposed approach is more general than the reference and is capable to reproduce the experimental data of this challenging benchmark, one adopts $K = 4.67kPa$, $G = 0.5kPa$, $n = 1$, $\alpha_i = 2$, $\gamma_{ij} = 4$, $R_1 = 200kPa$, $R_2 = 50kPa$, $R_3 = 1460kPa$ and different shear stiffness for fibers (shape effect) as: $R_{1(12)} = 80kPa$, $R_{1(13)} = 100kPa$, $R_{2(21)} = 80kPa$, $R_{2(23)} = 50kPa$, $R_{3(31)} = 500kPa$ and $R_{3(32)} = 100kPa$. In Fig. 16 results are compared with the experimental values given by Dokos et al. (2002) (adapted from Holzapfel and Ogden (2009)).

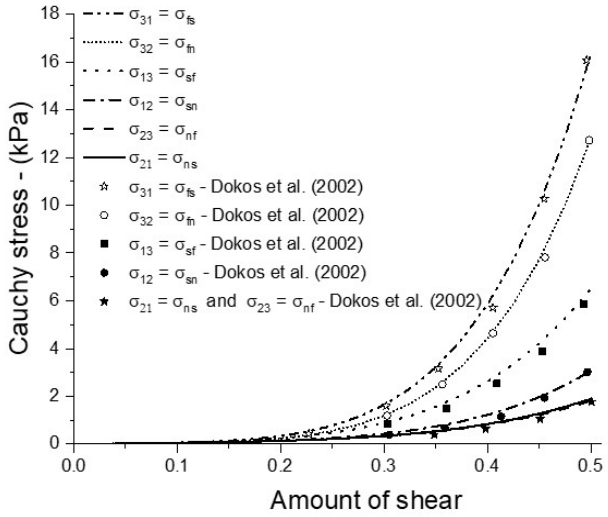

Figure 16 Comparing results of model (g) with experimental data presented by Doko et al (2002)

As one can see the proposed model(g), not based only on strain invariants, but taking advantage of the unified form (27) to provide spread fibers' stiffening, is able to reproduce numerical and experimental results of this challenging

biomechanical benchmark and can be used for practical purposes. In particular, comparing Figs. 15 and 16, one can see that the proposed model is able to reproduce the following experimental inequalities $\sigma_{31} \neq \sigma_{32}$, $\sigma_{21} \neq \sigma_{23}$ and $\sigma_{13} \neq \sigma_{12}$.

8 CONCLUSIONS

In the presented study, a unified expression to write large strains orthotropic elastic constitutive models was found. From this unified expression, it was verified that classical models based on strain invariants (which are difficult to interpret) can be replaced by models that have a direct connection with linear orthotropic elasticity expressions. From this finding, constitutive models that include longitudinal and transverse stiffening of spread fibers were proposed. Using these alternative models, an important biomechanical benchmark was successfully simulated, validating the proposal. In future works, it is intended to expand the formulation to consider random spreading of the fibers and nonlinear physical behavior (plasticity and/or damage) for both matrix and the fibers

ACKNOWLEDGMENTS

This research has been supported by the São Paulo Research Foundation, Brazil - Grant #2020/05393-4 and Coordenação de Aperfeiçoamento de Pessoal de Nível Superior - Brasil (CAPES) – Finance Code 001.

Author's Contributions: Conceptualization, HB Coda and RR Paccola; Methodology, HB Coda; Investigation, HY Hayashi, HB Coda and RR Paccola - original draft, HY Hayashi, HB Coda,RR Paccola; Writing - review & editing, HB Coda and RR Paccola; Funding acquisition, HY Hayashi and HB Coda; Resources, RR Paccola and HB Coda; Supervision, HB Coda.

Editor: Marco L. Bittencourt

References

Aguiar, A.R., Lopes da Rocha, G., (2018). On the Number of Invariants in the Strain Energy Density of an Anisotropic Nonlinear Elastic Material with Two Material Symmetry Directions. J Elast 131, 125–132. https://doi.org/10.1007/s10659-017-9642-5

Amores, V.J., San Millán, F.J., Ben-Yelun, I., Montáns, F.J., (2021). A finite strain non-parametric hyperelastic extension of the classical phenomenological theory for orthotropic compressible composites. Composites Part B: Engineering 212, 108591. https://doi.org/10.1016/j.compositesb.2020.108591.

Avazmohammadi, R., Soares, J.S., Li, D.S., Raut, S.S., Gorman, R.C., Sacks, M.S. (2019) A contemporary look at biomechanical models of myocardium, Annu. Rev. Biomed. Eng., 21, 417-442.

Balzani, D., Neff, P., Schröder, J., Holzapfel, G.A., (2006). A polyconvex framework for soft biological tissues. Adjustment to experimental data. International Journal of Solids and Structures 43 (20), 6052-6070. https://doi.org/10.1016/j.ijsolstr.2005.07.048

Bonet, J., Burton, A.J., (1998). A simple orthotropic, transversely isotropic hyperelastic constitutive equation for large strain computations. Comput. Methods Appl. Mech. Engrg. 162 (1-4), 151-164. https://doi.org/10.1016/S0045-7825(97)00339-3

Bonet, J., Wood, R., (1997). Nonlinear Continuum Mechanics for Finite Element Analysis, Cambridge University Press, New York.

Coda, H.B., (2021). An alternative finite strain elastoplastic model applied to soft core sandwich panels simulation. Latin American Journal of Solids and Structures 18 (6) e392, DOI10.1590/1679-78256568.

Coda, H.B., Greco, M., (2004). A simple FEM formulation for large deflection 2D frame analysis based on position description. Computer Methods in Applied Mechanics and Engineering 193 (33–35), 3541-3557. https://doi.org/10.1016/j.cma.2004.01.005.

Coda, H.B., Sanches, R.A.K., (2022). Unified solid–fluid Lagrangian FEM model derived from hyperelastic considerations. Acta Mech 233, 2653–2685. https://doi.org/10.1007/s00707-022-03237-z

Dokos, S., Smaill, B.H., Young, A.A., Le Grice, I.J., (2002). Shear properties of passive ventricular myocardium. Am. J. Physiol. Heart Circ. Physiol. 283, H2650–H2659. https://doi.org/10.1152/ajpheart.00111.2002

Ehret, A.E., Itskov, M., (2007). A polyconvex hyperelastic model for fiber-reinforced materials in application to soft tissues. J Mater Sci 42, 8853–8863. https://doi.org/10.1007/s10853-007-1812-6

Fallahi, H., Taheri-Behrooz, F., (2022) Phenomenological constitutive modeling of the non-linear loading-unloading response of UD fiber-reinforced polymers. Composite Structures 292, 115671.

Flory, P.J., (1961). Thermodynamic relations for high elastic materials. Transactions of the Faraday Society, 57, 829-838.

Gao, DY et al, (2022). Five-stage tensile constitutive model of hybrid fiber reinforced polymer bar, Journa of Building Engineering 58, 105006.

Gao J, Yang X, Guo J, Huang J, (2020)Hyperelastic mechanical properties of choppedara mid fiber-reinforced rubber composite under finite strain, Composite Structures, 243, 112187, ISSN 0263-8223, https://doi.org/10.1016/j.compstruct.2020.112187.

Gupta, A. et al, (2022) Homogenized modeling approach for effective property prediction of 3D-printed short fibers reinforced polymer matrix composite material. International Journal of Advanced Manufacturing Technology 118 (11-12), 4161-4178.

Hadjicharalambous, M., Chabiniok, R., Asner, L., Sammut, E., Wong, J., Carr-White, G., Lee, J., Razavi, R., Smith, N., Nordsletten, D., (2015). Analysis of passive cardiac constitutive laws for parameter estimation using 3D tagged MRI. Biomech Model Mechanobiol 14, 807–828. https://doi.org/10.1007/s10237-014-0638-9

Hartmann, S., Neff, P., (2003). Polyconvexity of generalized polynomial-type hyperelastic strain energy functions for near-incompressibility. International Journal of Solids and Structures 40 (11), 2767–2791. https://doi.org/10.1016/S0020-7683(03)00086-6

Holzapfel G.A., (2000). Nonlinear Solid Mechanics: A Continuum Approach for Engineering, Jhon Wiley & Sons, LTD.

Holzapfel, G.A., Ogden, R.W., (2009). Constitutive modelling of passive myocardium: a structurally based framework for material characterization, Phil. Trans. R. Soc. A 367, 3445–3475. https://doi.org/10.1098/rsta.2009.0091

Holzapfel, G.A., Ogden, R.W., (2010). Constitutive modelling of arteries. Proc. R. Soc. A 466, 1551–1597. https://doi.org/10.1098/rspa.2010.0058

Itskov, M., Khiêm, V.N., (2016). A polyconvex anisotropic free energy function for electro- and magneto-rheological elastomers. Mathematics and Mechanics of Solids 21 (9), 1126-1137. https://doi.org/10.1177/1081286514555140

Jadidi, M., Sherifova, S., Sommer, G., Kamenskiy, A., Holzapfel, G.A., (2021). Constitutive modeling using structural information on collagen fiber direction and dispersion in human superficial femoral artery specimens of different ages. Acta Biomaterialia 121, 461-474. https://doi.org/10.1016/j.actbio.2020.11.046.

Kishino, V.H., Kishino, R.T., Coda, H.B., (2022). A sequential investigation of the residual stresses and strains influence on the buckling of cold-formed thin-walled members. Thin-Walled Structures 180, 109814. https://doi.org/10.1016/j.tws.2022.109814

Latorre, M., Montáns, F.J., (2014). What-You-Prescribe-Is-What-You-Get orthotropic hyperelasticity. ComputMech 53, 1279–1298. https://doi.org/10.1007/s00466-013-0971-3

Lekhnitskii, S.G., (1963). Theory of Elasticity of an Anisotropic Body. 1st ed. Moscou: Mir, 430p.

Lubarda, V.A., Chen, M.C., (2018). On the elastic moduli and compliances of transversely Isotropic and orthotropic materials. Journal of Mechanics of Materials and Structures 3 (1), 153-171. http://dx.doi.org/10.2140/jomms.2008.3.153

Lv, H.D., Xie, W.J., Gao, W.Y., (2024). Nonlinear bond-slip model for fiber-reinforced polymer laminates externally bonded to thermally damaged concrete, Advances in Structural Engineering 27 (4), 585-605.

Mooney, M., (1940). A theory of large elastic deformation. Journal of Applied Physics, 11 (9), 582-592. https://doi.org/10.1063/1.1712836

Ogden, R.W., (1972). Large deformation isotropic elasticity – on the correlation of theory and experiment for incompressible rubberlike solids. Proc. R. Soc. Lond. A326565–584. http://doi.org/10.1098/rspa.1972.0026

Ogden, R.W., (1984). Non-linear Elastic Deformations. Ellis Horwood, New York.

Ogden, R.W., (1997). Non-linear elastic deformations. New York, NY: Dover.

Paccola, R.R., Coda, H.B., (2020). Alternative active nonlinear total Lagrangian truss finite element applied to the analysis of cable nets and long span suspension bridges. Latin American Journal of Solids and Structures, 17 (3) e268, DOI10.1590/1679-78255818.

Paccola, R.R., Sampaio, M.S.M., Coda H.B., (2015). Fiber-matrix Contact Stress Analysis for Elastic 2D Composite Solids. Latin American Journal of Solids and Structures 12 (3), 583-611. https://doi.org/10.1590/1679-78251282

Rivlin, R., Saunders, D., (1951). Large elastic deformations of isotropic materials VII. Experiments on the deformation of rubber. Philos. Trans. R. Soc. London Ser. A 243 (865), 251–288. https://www.jstor.org/stable/91489

Rubin, M.B., (2016). Seven Invariants Are Needed to Characterize General Orthotropic Elastic Materials: A Comment on [Shariff, J. Elast., 110:237–241 (2013)]. J Elast. 123, 253–254. https://doi.org/10.1007/s10659-015-9552-3.

Sampaio, M.S.M., Paccola, R.R., Coda, H.B., (2015). A geometrically nonlinear FEM formulation for the analysis of fiber reinforced laminated plates and shells. Composite Structures 119, 799-814. https://doi.org/10.1016/j.compstruct.2014.09.009.

Schröder, J., Neff, P., (2003). Invariant formulation of hyperelastic transverse isotropy based on polyconvex free energy functions. International Journal of Solids and Structures 40 (2), 401–445. https://doi.org/10.1016/S0020-7683(02)00458-4

Sharabi M, Varssano D, Eliasy R, Benayahu Y, Benayahu D, Ali R H, (2016) Mechanical flexure behavior of bio-inspired collagen-reinforced thin composites, Composite Structures, 153, 392-400, ISSN 0263-8223, https://doi.org/10.1016/j.compstruct.2016.06.031.

Shariff, M.H.B.M., (2013). Nonlinear Orthotropic Elasticity: Only Six Invariants are Independent. J Elast 110, 237–241. https://doi.org/10.1007/s10659-012-9389-y.

Shariff, M.H.B.M., (2022). A generalized strain approach to anisotropic elasticity. Sci Rep 12, 172. https://doi.org/10.1038/s41598-021-03842-3

Soares H.B., Paccola, R.P., Coda, H.B., (2021). A conjugate modal force strategy for instability analysis of thin-walled structures: an unconstrained vector positional finite element approach, Latin American Journal of Solids and Structures, 18 (2) e344, DOI10.1590/1679-78256253

Spencer, A.J.M., (1971). Theory of invariants, in Continuum Physics, In: Vl, Eringen, A.C., Ed., Academic Press, New York, 239-253.

Spencer, A.J.M., (1984). Constitutive theory for strongly anisotropic solids. In: Spencer, A.J.M. (ed.) Continuum Theory of the Mechanics of Fiber Reinforced Composites. CISM Courses and Lectures, vol. 282, pp. 1–32.

Sussman, T., Bathe, K.J., (2009) A model of incompressible isotropic hyperelastic material behavior using spline interpolations of tension–compression test data. Commun Number Method Eng 25 (1), 53–63. https://doi.org/10.1002/cnm.1105

Yang H, Yao X-F, Yan H, Yuan Y-N, Dong Y-F, Liu Y-H, (2018), Anisotropic hyper-viscoelastic behaviors of fabric reinforced rubber composites, Composite Structures, 187, 116-121, ISSN 0263-8223, https://doi.org/10.1016/j.compstruct.2017.12.026.

Zhang L, Sertse H M, Yu W, (2019) Variational asymptotic homogenization of finitely deformed heterogeneous elastomers, Composite Structures, 216, 379-391, ISSN 0263-8223, https://doi.org/10.1016/j.compstruct.2019.02.066.

Zhao DB et al, (2023) Effects of scale and strain rate on the tensile behaviors of large-rupture-strain fiber-reinforced polymers (LRS-FRP), Construction and Building Materials, vol 380, 131267.

Appendix A: List of symbols and abbreviations (in order of appearance)

FEM – Finite Element Method
SVK – Saint-Venant- Kirchhoff
$\mathbf{C}$ - Cauchy-Green right stretch tensor
Det - Determinant of a tensor
$\mathbf{A}$ - Deformation Gradient
W - Specific strain energy
J - Jacobian – determinant of the deformation gradient
$\mathbf{E}$ - Green-Lagrange strain
$\mathbf{I}$ - Identity tensor of order 2
$\overline{\mathbf{A}}$ - Isochoric part of the deformation gradient
$\hat{\mathbf{A}}$ - Volumetric part of the deformation gradient
$\overline{\mathbf{C}}$ - Isochoric part of the Cauchy-Green stretch
$\hat{\mathbf{C}}$ - Volumetric part of the Cauchy-Green stretch
$\hat{W}$ - Volumetric part of specific strain energy
$\overline{W}$ - Isochoric part of specific strain energy
$\overline{\mathbf{E}}$ - Isochoric part of the Green-Lagrange strain
K - Bulk modulus
n - Volumetric strain energy controlling paramenter
$\mathbf{D}$ - Inverse of the Cauchy-Green stretch
$\hat{\boldsymbol{S}}$ - Volumetric part of the second Piola Kirchhoff stress
$\overline{\boldsymbol{S}}$ - Isochoric part of the second Piola Kirchhoff stress
$\hat{\mathfrak{H}}$ - Volumetric part of the tangent constitutive stiffness tensor
$\hat{\mathfrak{H}}^0$ - Volumetric part of the tangent constitutive stiffness tensor at zero strain
$\overline{\mathfrak{H}}$ - Isochoric part of the tangent constitutive stiffness tensor
W^* - Usual strain energy function without imposing isochoric behavior
$\vec{o}^i$ - Orthotropic direction i
T_{ijk} - Invariant vector $\vec{T}$ belonging to plane jk
Tr - Trace of a second order tensor
I_i - Invariants of the right Cauchy stretch tensor
$\overline{I}_i$ - Invariants of the right Cauchy stretch tensor isochoric part
$\hat{I}_i$ - Invariants of the right Cauchy stretch tensor volumetric part
$\overline{R}$ - General value for each model that controls the normality condition
a_i - General elastic constants of unified specific strain energy function
$\overline{m}_i$ - Elastic constants of specific strain energy of model (a)
k_i - Elastic constants of specific strain energy of model (b)
μ_i - Elastic constants of specific strain energy of model (c)
β_i - Elastic constants of specific strain energy of model (c)
λ - Elastic constants of specific strain energy of model (c)
α_i - Elastic constants of specific strain energy of model (c) or power strains of model (g)
δ_{ij} - Kronecker delta
G - Shear elastic modulus
γ_{ij} - Power of strains in model (g)

$G_{i(i\ell)}$ - Shear modulus of fibers i in direction ℓ.

$a_{(i)}^{fibers}$ - Total fiber area crossing plane i

$a_{(i)}^{cont}$ - total area of plane i

R_i - Longitudinal relative stiffness of fibers in direction i

$R_{i(i\ell)}$ - Shear relative stiffness of fibers i in direction ℓ

Π - Total mechanical energy

ρ_0 - Lagrangean density

$\vec{y}$ - Current position of a point inside the continuum

$\ddot{\vec{y}}$ - Acceleration of a point inside the continuum

$\vec{b}^0$ - Body force mapped in the initial configuration acting I current configuration

$\vec{p}^0$ - Surface force mapped in the initial configuration acting I current configuration

$\vec{x}$ - Initial position of a point inside the continuum

$\vec{f}$ - Change of configuration or deformation

ϕ - Finite Element shape function

$\vec{Y}$ - Current nodal position vector

$\vec{X}$ - Initial nodal position vector

$\vec{\xi}$ - Dimensionless coordinates – mapping

$\vec{B}^0$ - nodal values of body force

$\vec{P}$ - Nodal values of surface forces

$\ddot{\vec{Y}}$ - Nodal Acceleration vector

$\vec{F}^{\text{int}}$ - Internal forces written at nodal positions

$\vec{F}^{ext}$ - External forces at nodal positions

L_0 - Initial length of fiber element

L - Current length of fiber element

$\mathbb{E}$ - Longitudinal elastic modulus for fiber elements

w_{SVK} - Saint-Venant-Kirchhoff specific strain energy for fiber element

w_{AL} - Almansi specific strain energy for fiber element

W_{SVK} - Strain energy of a fiber element - Saint-Venant-Kirchhoff

W_{AL} - Strain energy of a fiber element - Almansi

W^{ℓ} - Strain energy of a fiber ℓ it can be W_{AL} or W_{SVK}

$\vec{\xi}^{\,p}$ - Dimensionless coordinate for an immersed point

$f_{\gamma}^{\text{int}\,\alpha}$ - Internal force of a fiber element

$\mathbf{\Psi}_{i\gamma}^{p\alpha}$ - Fiber internal force weight

$\boldsymbol{H}$ - Hessian matrix

Appendix B: In order to be complete, this appendix shows the usual linear elastic compliance and stiffness constants used in parts of this study (Lekhnitskii, 1963). The following equationis the adaptation from orthotropic Hooke's Law to the Saint-Venant-Kirchhoff-like model for orthotropic material using the Voigt's notation.

$$\begin{Bmatrix} E_{11} \\ E_{22} \\ E_{33} \\ E_{12} \\ E_{13} \\ E_{23} \end{Bmatrix} = \begin{bmatrix} 1/E_1 & -\nu_{12}/E_2 & -\nu_{13}/E_3 & 0 & 0 & 0 \\ -\nu_{21}/E_1 & 1/E_2 & -\nu_{23}/E_3 & 0 & 0 & 0 \\ -\nu_{31}/E_1 & -\nu_{32}/E_2 & 1/E_3 & 0 & 0 & 0 \\ 0 & 0 & 0 & 1/2G_{23} & 0 & 0 \\ 0 & 0 & 0 & 0 & 1/2G_{13} & 0 \\ 0 & 0 & 0 & 0 & 0 & 1/2G_{12} \end{bmatrix} \begin{Bmatrix} S_{11} \\ S_{22} \\ S_{33} \\ S_{23} \\ S_{13} \\ S_{12} \end{Bmatrix} \tag{A1}$$

in which, by symmetry, $E_i\nu_{(i)j} = E_j\nu_{(j)i}$ for ν_2. In this representation, the number of elastic constants is 9, i.e., three longitudinal elastic moduli E_1, E_2 and E_3; three shear elastic moduli G_{12}. G_{13} and G_{23}; and three Poison ratio ν_{12}, ν_{13} and ν_{23}. The terms of the constitutive elastic tensor of Eq. (34) are given explicitly by:

$$\mathfrak{H}^0_{1111} = E_1\left(1-\nu_{23}\nu_{32}\right)/\Delta \tag{A2}$$

$$\mathfrak{H}^0_{1122} = \mathfrak{H}^0_{2211} = E_2\left(\nu_{23}\nu_{31}+\nu_{21}\right)/\Delta = E_1\left(\nu_{13}\nu_{32}+\nu_{12}\right)/\Delta \tag{A3}$$

$$\mathfrak{H}^0_{1133} = \mathfrak{H}^0_{3311} = E_1\left(\nu_{12}\nu_{23}+\nu_{13}\right)/\Delta = E_3\left(\nu_{21}\nu_{32}+\nu_{31}\right)/\Delta \tag{A4}$$

$$\mathfrak{H}^0_{2222} = E_2\left(1-\nu_{13}\nu_{31}\right)/\Delta \tag{A5}$$

$$\mathfrak{H}^0_{2233} = \mathfrak{H}^0_{3322} = E_2\left(\nu_{13}\nu_{21}+\nu_{23}\right)/\Delta = E_3\left(\nu_{31}\nu_{12}+\nu_{32}\right)/\Delta \tag{A6}$$

$$\mathfrak{H}^0_{3333} = E_3\left(1-\nu_{12}\nu_{21}\right)/\Delta \tag{A7}$$

$$\mathfrak{H}^0_{1212} = 2G_{12} \tag{A8}$$

$$\mathfrak{H}^0_{1313} = 2G_{13} \tag{A9}$$

$$\mathfrak{H}^0_{2323} = 2G_{23} \tag{A10}$$

$$\Delta = \left(1-\nu_{23}\nu_{32}\right)-\nu_{12}\left(\nu_{21}+\nu_{23}\nu_{31}\right)-\nu_{13}\left(\nu_{21}\nu_{32}+\nu_{31}\right) \tag{A11}$$

Positioned in Voigt's notation as:

$$\mathfrak{H} = \begin{bmatrix} \mathfrak{H}^0_{1111} & \mathfrak{H}^0_{1122} & \mathfrak{H}^0_{1133} & 0 & 0 & 0 \\ & \mathfrak{H}^0_{2222} & \mathfrak{H}^0_{2233} & 0 & 0 & 0 \\ & & \mathfrak{H}^0_{3333} & 0 & 0 & 0 \\ & & & 2\mathfrak{H}^0_{2323} & 0 & 0 \\ & Sym & & & 2\mathfrak{H}^0_{1313} & 0 \\ & & & & & 2\mathfrak{H}^0_{1212} \end{bmatrix} \tag{A12}$$